Edelweiss Applied Science and Technology
ISSN: 2576-8484
Vol. 9, No. 7, 1748-1784
2025
Publisher: Learning Gate
DOI: 10.55214/2576-8484.v9i7.9008

Hybrid systems in buildings: Control strategies for optimal integration

Abdoul-Razak Ali-Tagba[1,2], Mazabalo Baneto[1,2*], Arash Takshi[3], Dumitru Dorin Lu-cache[4]
[1]Centre d'Excellence Régional pour la Maîtrise de l'Electricité (CERME), University of Lome, 01BP1515 Lome, Togo; mazbaneto@gmail.com (M.B.).
[2]Department of Physics, Solar Energy Laboratory, University of Lome, 01BP1515 Lome, Togo.
[3]Department of Electrical Engineering, University of South Florida, 4202 E Fowler Ave, Tempa, FL, 33620, USA.
[4]Faculty of Electrical Engineering, "Gheorghe Asachi" Technical University of Iaşi, 700050 Iasi, Romania.

Abstract: This study proposes an optimized control strategy for a hybrid photovoltaic–wind system with battery storage, designed for off-grid applications. The objective is to enhance energy stability and overall efficiency through an adaptive fuzzy logic-based MPPT controller. The methodological approach is based on multi-component modeling using MATLAB/Simulink, integrating a multi-port DC converter and parametric optimization functions. The results demonstrate an overall energy efficiency of 92.7%, a 22% reduction in power oscillations compared to the conventional P&O algorithm, and DC bus voltage stabilization within ±0.5%. Furthermore, power supply continuity reaches 98.7%, and total harmonic distortion remains below 3.2%. The hierarchical energy management strategy ensures that the battery state of charge is maintained between 30% and 90%. These performance outcomes suggest that the proposed architecture is well-suited for autonomous microgrids in remote areas. Practical implications include the optimization of hybrid systems for sustainable electrification.

Keywords: *Current control strategy, Energy management, Hybrid renewable energy systems, Multi-port converter, Photovoltaic and wind energy.*

1. Introduction

Due to the increasing demand for energy and environmental, economic, and political problems associated with the use of fossil energy resources, renewable energy sources are becoming an essential alternative for energy production [1]. Today, renewable energy sources have many advantages, including sustainability and low pollution [2, 3]. Wind and photovoltaic (PV) technologies are two examples of renewable energy systems that have the potential to replace conventional energy production systems [4, 5].

On the other hand, due to the recent decline in solar panel prices, it is currently estimated that installed photovoltaic capacity will reach 800 GW by 2030 [6]. Experts have predicted that by 2050, wind and photovoltaic power will account for about 50% of all electricity generated worldwide [7, 8]. However, one of the main problems with these two sources is their random and intermittent nature, which makes it difficult to control their individual uses. To mitigate the problem, one approach is to use a hybrid system with wind and solar energy sources equipped with an energy storage unit. These hybrid systems have recently attracted the interest of many researchers working in the fields of renewable energy sources [9, 10]. Three hybrid system topologies have been proposed: common DC-BUS, common AC-BUS and combined common AC/DC-Bus [11]. In general, these topologies require the use of a number of power converters and controllers to adapt and facilitate the transition of energy produced from renewable sources to the end use, which adds to the total complexity of the system.

Moreover, as the number of converters increases, the system efficiency decreases due to losses in each converter [12]. Efficient control of converters with a constant and optimal switching frequency

History: Received: 21 May 2025; Revised: 1 July 2025; Accepted: 4 July 2025; Published: 22 July 2025
* Correspondence: mazbaneto@gmail.com

helps to minimize the heating of power components [13]. In this paper, the structure of the studiedhybrid system is composed of two power sources (photovoltaic and wind), a storage system, a multi-port DC converter, a DC/AC converter and loads as presented in Figure 1.

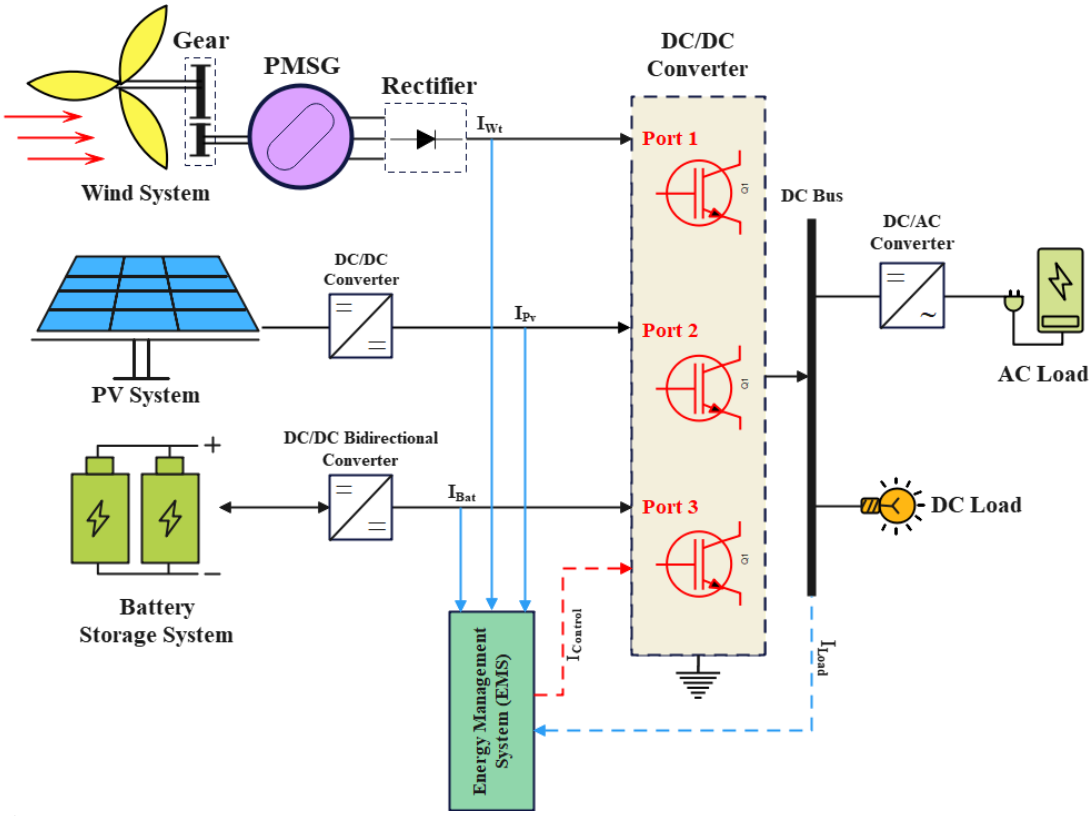

Figure 1.
Architecture of the control strategy of the wind-PV system with batteries.

The objective of this study is to design an adaptive current control system for multi-port DC converters, capable of efficiently managing load variations and external disturbances while maintaining optimal system stability. This approach aims to ensure accurate and reliable power distribution among the different ports of the converter, thus optimizing energy efficiency and improving overall system performance. In addition, maximum power point tracking strategies have been applied to photovoltaic and wind sources to ensure optimal system operation. Part of the energy control strategy is based on the fuzzy logic approach.

Many PV and wind system models and designs have been developed using different approaches. The design can be classified into two categories: grid-based or stand-alone. Researchers like Hassan, et al. [14] show that the operation of PV/wind hybrid systems, with different topologies, can be used for hybridization of more than one system; the advantages and disadvantages of using such systems have been studied by Chrifi-Alaoui, et al. [15]. The stability of grid-connected systems with hybrid storage [16] and real-time testing of off-grid systems for rural electrification [17]. These studies highlight the technical benefits, operational challenges, and performance criteria of hybrid systems.

Also in the literature, many different control strategies have been considered. The PV/wind hybrid system was used by Dihrab and Sopian [18]to generate electricity in Iraq. The planned system was simulated using the Matlab solver, the final results showed that it is possible to use such a system as a cold start energy source during a total shutdown period. Hybrid PV/wind systems have been

Edelweiss Applied Science and Technology
ISSN: 2576-8484
Vol. 9, No. 7: 1748-1784, 2025
DOI: 10.55214/2576-8484.v9i7.9008

extensively researched to optimize their performance for diverse energy applications. Amoussou, et al. [19] developed an integrated design combining solar, wind, lithium battery storage, and hydrogen production to replace a heavy fuel oil power plant, demonstrating the system's sustainability and efficiency. Concurrently, advanced modeling approaches including an innovative topology combining Cuk and SEPIC converters simulated in MATLAB have significantly enhanced the performance metrics of hybrid PV/wind systems [20].

Energy control is a critical component, as highlighted by a study on a solar-wind hybrid system coupled with lead-acid batteries, which underscores the importance of effective management to ensure power supply stability and reliability. Although small-scale microgeneration remains underexplored, Australia's Bushlight project exemplifies the potential of standalone renewable systems to successfully electrify remote communities, providing valuable operational insights [21].

For residential applications, Aissi, et al. [22] validated the feasibility of an optimized PV/wind hybrid system tailored to specific climatic conditions, demonstrating its energy efficiency and local adaptability. Systems with basic MPPT (Maximum Power Point Tracking), despite their simplicity, remain practical, reliable, and cost-effective solutions for diverse applications. Regarding grid integration, Al Shereiqi, et al. [23] proposed hybrid system sizing optimization to mitigate generation variability and enhance national grid stability. Finally, in off-grid rural areas, optimal sizing methodologies based on genetic algorithms have reduced costs for standalone PV/wind systems, confirming their economic superiority over single-source alternatives.

A research conducted by Mohammadi, et al. [24] used the particle swarm optimization (PSO) algorithm for the optimal sizing of PV and wind systems, although the study was limited to a microgrid system, but energy storage was included. Askarzadeh [25] used the discrete chaotic harmony search based simulated annealing (SA) algorithm for the optimal design of a PV/wind hybrid system. The suggested method is used to obtain the best possible design of a PV/wind hybrid system. The simulation results show the outstanding efficiency of the SA algorithm. The optimization study conducted by Merei, et al. [26] focuses on off-grid PV/Wind hybrid using different battery technologies based on the genetic algorithm (GA) and has been successfully implemented. An optimal control strategy based on an adaptive predictive model for a solar hybrid system (PV + BESS) was developed by AbdElrazek, et al. [27]. The controller regulates production and storage to follow the power setpoints, while respecting the system constraints and ensuring sufficient energy reserves.

In a context of accelerated energy transition, this study proposes a significant methodological advance in intelligent energy management in renewable hybrid systems. Unlike classic fuzzy control architectures, it introduces a dynamic and adaptive rule base, comprising 25 rules – compared to 9 to 15 in previous studies [28, 29] as well as an asymmetric membership function of type A. This configuration allows a measured reduction of power oscillations of the order of 22% compared to conventional Perturb and Observe (P&O) techniques, as illustrated in Figure 22. It also guarantees a better dynamic reactivity (±0.2 s) in the face of rapid fluctuations in sunlight (>100 W/m²/s), a critical scenario still little explored in the scientific literature [30, 31].

Furthermore, recent technological advances in photovoltaic and wind power, combined with the continued rise in fossil fuel costs, are strengthening the economic viability of hybrid renewable energy systems. With this in mind, the study proposes a simplified model of a stand-alone hybrid system – not connected to the grid – integrating intelligent energy management algorithms. These algorithms ensure optimized maximum power point tracking (MPPT) from renewable sources, while maintaining the stability of the electrical system under variable environmental conditions. The developed architecture thus constitutes a relevant contribution to the energy optimization of stand-alone microgrids and the resilience of energy infrastructures in areas with limited access to the grid.

This article begins with the "Materials and Methods" section, where the theoretical models and components of the hybrid system studied are presented. This part details the different components of the system and the methodology adopted to carry out the simulations. The "Results and Discussion" section then highlights the simulations carried out on the autonomous hybrid system. The results

Edelweiss Applied Science and Technology
ISSN: 2576-8484
Vol. 9, No. 7: 1748-1784, 2025
DOI: 10.55214/2576-8484.v9i7.9008

obtained are analyzed and discussed, taking into account the system performance and their comparison with previous studies. Finally, the Conclusion summarizes the main elements of the study, recalls the major contributions and proposes perspectives for future work.

2. Materials and Methods

According to a thorough literature review, many studies are underway, with divergent ideas and needs, on the possibility of integrating wind and photovoltaic systems. These studies can be classified into three categories: modeling, design, optimization, control, and techno-economic strategies. Some researchers have proposed a stand-alone hybrid system, while others have applied a wind and photovoltaic system in grid-connected mode. In this work, the study focuses on the multi-point management strategy of the Hybrid Renewable Energy System (HRES), presented in Figure 1. The mathematical modeling of the proposed system is as follows:

2.1. Modeling of the Wind System

Wind energy, one of the most abundant resources, is the second fastest-growing renewable energy technology in the world. This part of the wind system consists of a horizontal-axis turbine, a permanent magnet generator, and a diode rectifier to convert alternating current to direct current, a DC/DC switch, and an MPPT controller to track and calculate the MPP. Figure 2 shows the block diagram of the system used for modeling. Its model is as follows:

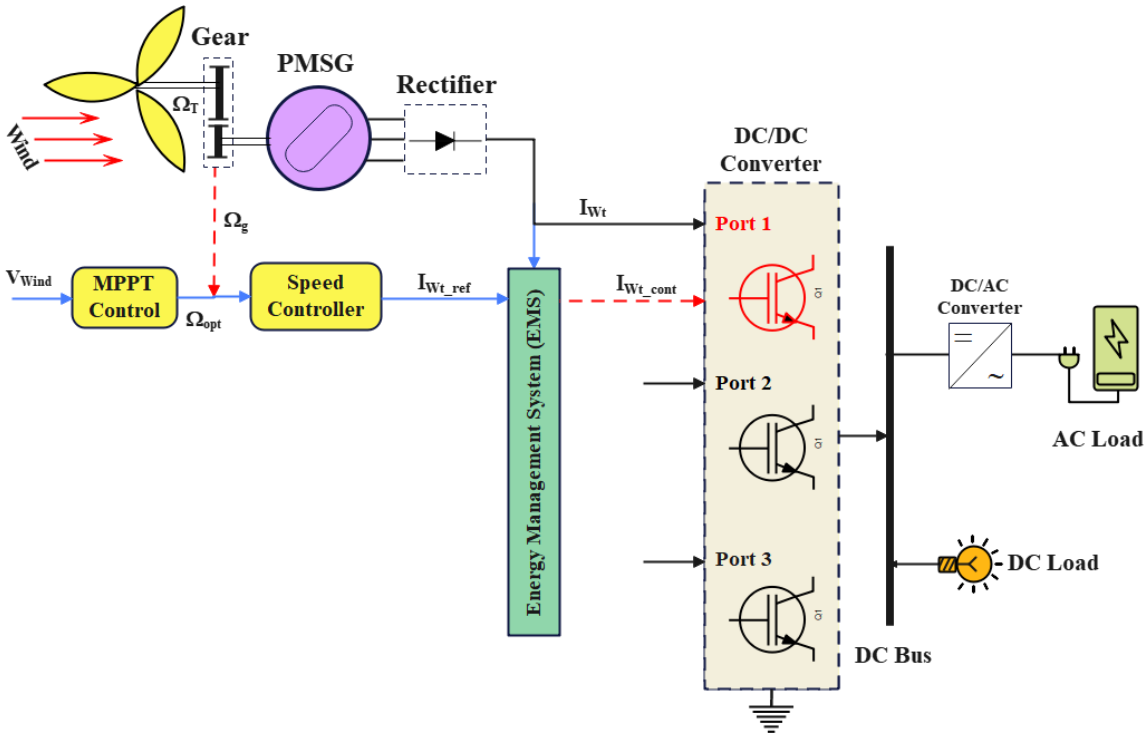

Figure 2.
The wind system.

2.1.1. Turbine Model

The power developed by the wind comes from the wind turbine and is defined by equation (1) [32]:

$$P_{Wt} = \frac{1}{2}.\rho.A.V^3.C_p(\lambda,\beta) \quad (1)$$

Edelweiss Applied Science and Technology
ISSN: 2576-8484
Vol. 9, No. 7: 1748-1784, 2025
DOI: 10.55214/2576-8484.v9i7.9008

Where P_{Wt} [Watt]: aerodynamic power of the turbine; ρ [Kg/m³]: air density; A [m²]: surface area of the turbine blade; V [m/s]: wind speed; C_p: coefficient of performance or efficiency of the turbine; β: blade inclination angle [degree]; λ: tip speed ratio.

The tip speed ratio λ is the ratio of the linear speed of the blades to the wind speed, and it is represented by equation (2):

$$\lambda = \frac{\Omega_g R}{V} \tag{2}$$

Where Ω_g: rotor rotation speed in [rad/sec], R: radius of the blades [m].

The gear ratio G is employed between the turbine and the generator to increase the rotational speed. This relationship is described by equation (3):

$$G = \frac{\Omega_g}{\Omega_T} = \frac{T_T}{T_m} \tag{3}$$

Where Ω_T: turbine speed in [rad/sec], T_T: turbine torque [N.m], T_m: Torque applied to the generator [N.m].

In the existing literature Saget [32]; Abdin and Xu [33]; Patel and Beik [34] and Reddy, et al. [35] numerous formulations are provided for the calculation of the power coefficient C_p. For the present case study, with the assumption that the angle β = 0, the value of C_p is expressed by the following equation (4):

$$C_P = -0{,}7317\lambda^3 + 0{,}2953\lambda^2 + 0{,}8760\lambda \tag{4}$$

The mechanical equation is expressed by equation (5):

$$\frac{d\Omega}{\mathrm{dt}} = -\frac{1}{\mathrm{J}}(T_m - |T_{em}| - f.\Omega) \tag{5}$$

Where Ω: rotation speed; J: total inertia of the turbine; T_{em}: electromagnetic torque produced by the generator; T_m: torque of the multiplier; f: coefficient of friction.

Figure 3 shows the interconnection between the scheme of equations (1) to (5).

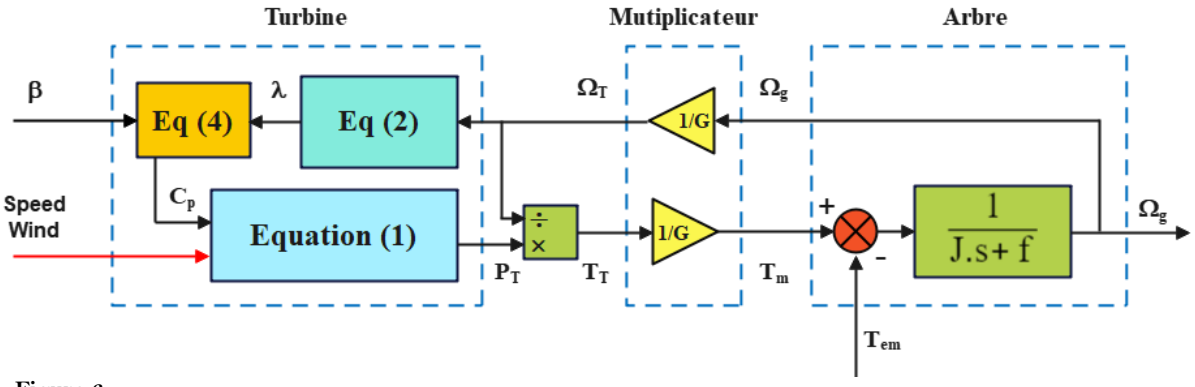

Figure 3.
Block diagram of the wind turbine model.

Edelweiss Applied Science and Technology
ISSN: 2576-8484
Vol. 9, No. 7: 1748-1784, 2025
DOI: 10.55214/2576-8484.v9i7.9008

2.1.2. Permanent Magnet Synchronous Generator (PMSG) Modeling

The permanent magnet rotor wind turbine (PMSG) was chosen for this study because of its high efficiency and high torque. The amplitude and frequency of the voltage induced by the PMSG vary with the wind speed. In order to overcome this problem, the generated power will be converted into direct current using a rectifier [36]. The mathematical equations of PMSG are given in a synchronous framework by the following equation (6):

$$\begin{cases} V_d = -R_s I_d - L_d \dfrac{dI_d}{dt} + L_q \omega I_q \\ V_q = -R_s I_q - L_q \dfrac{dI_q}{dt} - L_d \omega I_d + \phi_f \omega \\ T_{em} = -\dfrac{3}{2} p \phi_f L_q \end{cases} \quad (6)$$

Where Rs is the stator resistance, ω is the rotor electrical speed (ω = pΩ), I_d, I_q, V_d, V_q, L_d, L_q, are respectively the direct and quadrature components of the stator current, voltage and inductance and ϕ f is the permanent magnet flux.

2.1.3. MPPT Wind Controller

The literature presents many MPPT techniques for wind systems. In this work, the speed-to-peak ratio control presented in Figure 4 is used. The optimal speed is calculated from the optimal speed-to-peak ratio λ_{opt} and wind speed, as shown in equation (7).

$$\Omega_{opt} = \frac{\lambda_{opt}}{R}.V \quad (7)$$

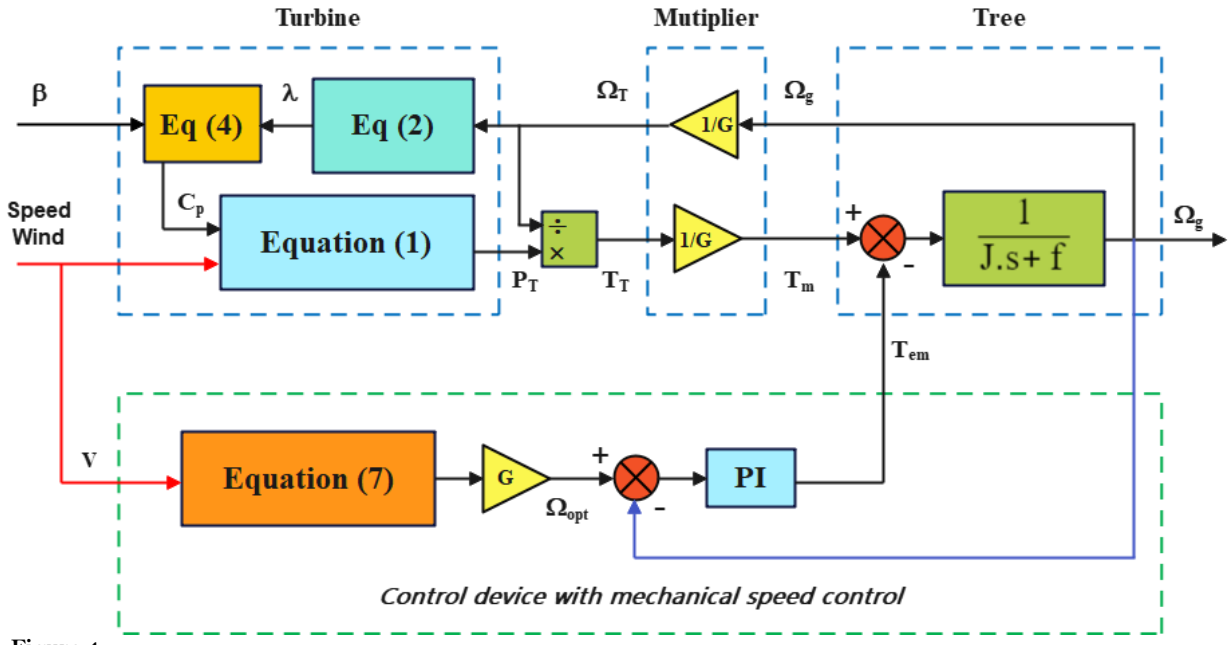

Figure 4.
Functional diagram of maximum power extraction from a wind turbine.

The wind system parameter data are in Table 1 below.

Edelweiss Applied Science and Technology
ISSN: 2576-8484
Vol. 9, No. 7: 1748-1784, 2025
DOI: 10.55214/2576-8484.v9i7.9008

Table 1.
Wind system parameters.

Description	***Value***
Radius R	0.62 m
Air density	1.25 kg/m^3
Gear ratio G	20 A
Permanent magnet flux	0.06 Wb
Stator inductances Ld = Lq	10 mH
Stator resistance Rs	0.0675 Ω
Pole numbers p	3
Total inertia, J	0.00176 kg.m^2
Friction coefficient	0.38×10^{-4} (SI)
Optimal Tip-Speed Ratio	0.78
Maximum power coefficient C_{pmax}	0.515

With a global approach, the electrical power generated by the wind turbine can be formulated proportionally to the area swept by its rotor (A_{wt}) by equation (8) [37]:

$$PG_{Wt} = \frac{1}{2}\eta_{gb}.\eta_g.C_p.\rho.A_{Wt}.V^3 = \frac{1}{2}\eta_t.\rho.A_{Wt}.V^3 \quad (8)$$

Where ρ [kg/m^3] represents the air density present in the atmosphere, V [m/s] denotes the wind velocity, A_{wt} [m^2] is the area swept by the wind turbine rotor, and C_p is the energy Where ρ [Kg/m^3]: is the density of air available in the atmosphere; V [m/s]: the wind speed; A_{wt} [m^2]: the surface swept by the wind turbine rotor; C_p: is the energy conversion coefficient or the efficiency of the turbine; η_{gb}: the efficiency of the speed variator; η_g : the efficiency of the generator; $\eta_t = C_p \times \eta_{gb} \times \eta_g$: Overall efficiency assumed to be 30% for three-bladed horizontal axis wind turbines [38].

For equation (8) to be linear, it is necessary that the wind turbines constituting the system have a uniform efficiency. This linearization is acceptable for small domestic wind turbines, with close optimal power factors for swept areas ranging from 1 to 25 m^2. The nominal power is assumed to be reached at a wind speed of 12 m/s and remains constant beyond this threshold. This consideration does not fix a type of wind turbine and therefore makes the proposed optimization method more general.

2.2. Modeling of the Photovoltaic System

Photovoltaic energy is produced from solar radiation using semiconductor materials. The system configuration is shown in Figure 5.

Edelweiss Applied Science and Technology
ISSN: 2576-8484
Vol. 9, No. 7: 1748-1784, 2025
DOI: 10.55214/2576-8484.v9i7.9008

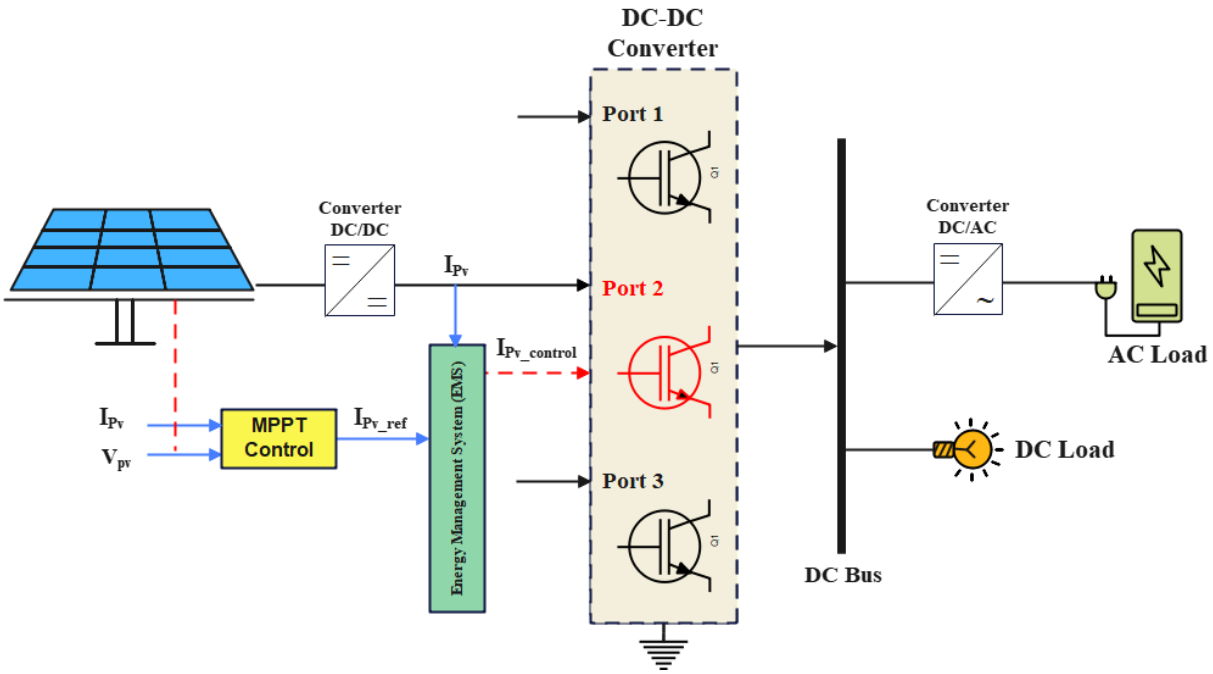

Figure 5.
The photovoltaic solar system.

2.2.1. Photovoltaic Panel Model

A large number of models describing the behavior of photovoltaic solar panels can be found in the literature [39, 40]. The most widespread is the single diode model, shown in Figure 6. It indicates that a photonic current source I_{ph} is connected to a parallel diode. Here, R_s is a series resistance, R_p is connected in parallel, while R_L is the load resistance. The reverse saturation current of the diode is I_s. The resistance R_p is very high compared to Rs. The anode current of the diode V d and the cell voltage V_{pv} can be obtained [41] by applying Kirchhoff's law (KCL) to the equivalent circuit of the solar cell with equations (9), (10) and (11):

$$I_{ph,source} - I_d - \frac{V_d}{R_{sh}} - I_{pv} = 0 \tag{9}$$

$$I_d = I_{sat}\left[exp\left(\frac{qV_d}{nk_BT}\right) - 1\right] \tag{10}$$

$$V_d = V_{pv} + R_s I_{pv} \tag{11}$$

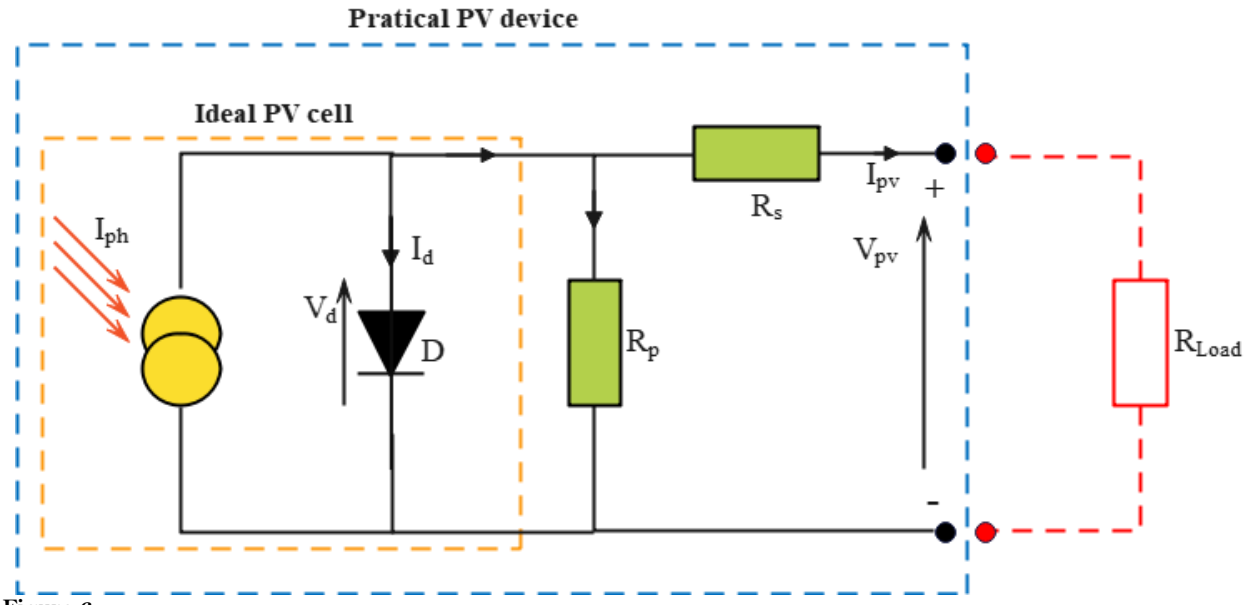

Figure 6.
Equivalent circuit of a single diode PV photovoltaic cell.

If A_{pv} expressed in m² is the surface area of the module and I_{rr} illumination in W/m², the electrical power generated by the PG_{pv} photovoltaic panels is given by equation (12) [42]:

$$PG_{pv} = \eta_{pv} \times A_{pv} \times I_{rr} \quad (12)$$

With, η_{pv}: overall efficiency of the module, it is given by equation (13) [43, 44]:

$$\eta_{pv} = \eta_r \times \eta_{pc} \times [1 - \beta_t(T_c - T_{NOCT})] \quad (13)$$

This formula takes into account the following parameters:

η_r: Reference efficiency of the photovoltaic module. It is defined as the ratio between the maximum power produced and the power of solar radiation reaching the module. It depends on the technology used. Polycrystalline silicon modules were chosen for the study, with an efficiency of approximately 13%.

η_{pc}: degradation factor. It takes into account the operating point of the modules, which is rarely optimal, and which can be aggravated by the degradation of the characteristics of the modules or their performance over time (aging and dust deposition). Here, η_{pc} will be equal to 0.9 [45].

β_t: coefficient of influence of the temperature of the photovoltaic cells on the generator's efficiency, between 0.004 and 0.006 per degree Celsius.

T_c: cell temperature [°C]. For a polycrystalline silicon photovoltaic module, it can be estimated from the ambient temperature T_a [°C] and the solar irradiation I_{rr}, using equation (14) [44]:

$$T_c = 30 + 0{,}0175 \times (I_{rr} - 300)] + 1{,}14 \times (T_a - 25) \quad (14)$$

T_{NOCT}: Nominal Operating Temperature of the Cell. It is defined as the temperature reached by the cell in its module in open circuit, under a sunshine of 800 W/m², an ambient temperature of 25 °C and a wind of 1 m/s. The commonly encountered values are between 40 and 50 °C. For this work, after consulting the technical data of different polycrystalline silicon modules, a typical value of T_{NOCT} equal to 45 °C and a typical value of β_t of 0.0045 per degree Celsius were considered. The data of the PV module used are presented in Table 2.

Edelweiss Applied Science and Technology
ISSN: 2576-8484
Vol. 9, No. 7: 1748-1784, 2025
DOI: 10.55214/2576-8484.v9i7.9008

Table 2.
Parameters of photovoltaic modules.

Description	***Value***
Maximum Power (P_{max})	105 W
Voltage at P_{max} (V_{mp})	24 V
Current at P_{max} (I_{mp})	4.4 A
Open Circuit Voltage (V_{oc})	32 V
Short Circuit Current (I_{sc})	5 A

The voltage-current (V-I) and voltage-power (V-P) characteristics according to equation (9) are given in Figure 7.

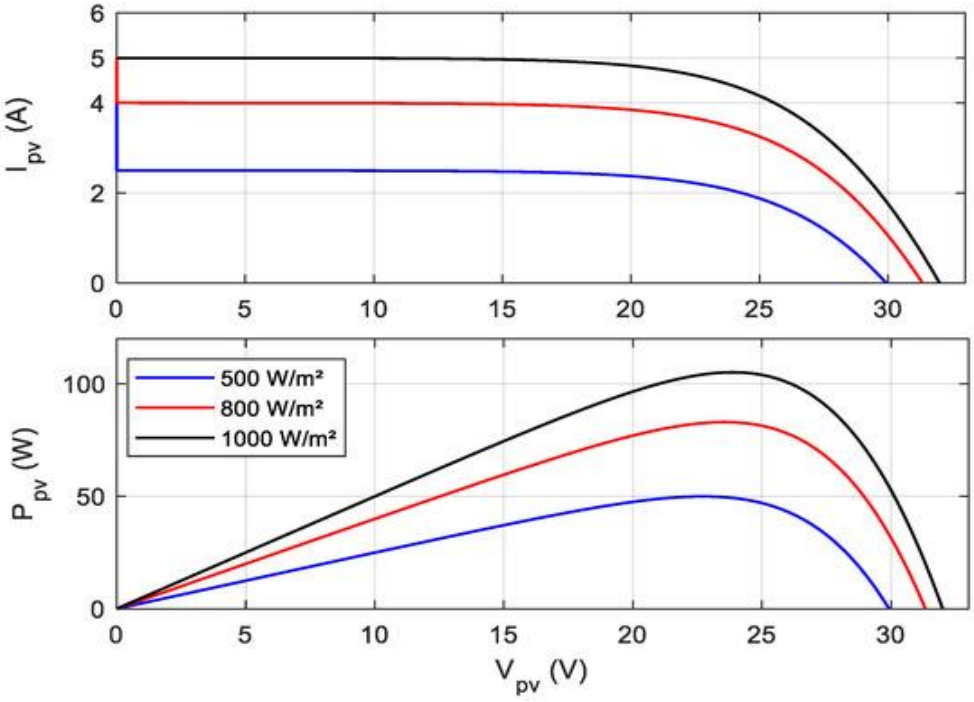

Figure 7.
V-I and V-P characteristics of the photovoltaic panel.

2.2.2. Fuzzy Logic MPPT Controller

The MPPT controller developed in this study is based on an optimized fuzzy logic approach, aiming to improve the energy efficiency of stand-alone photovoltaic systems. Unlike conventional methods, this controller integrates a dynamic self-adjustment mechanism of gains (Eq. (17– (18inspired by the work of Mudi and Pal [46] allowing real-time adaptation of the defuzzification parameters according to the state of charge (SOC) of the battery. This adaptive capability contributes to minimizing the 12% energy losses observed during the transition phases between the charging and discharging modes, as detailed in section 3.3.

The implemented MPPT method is thus based on fuzzy logic, recognized for its robustness in the face of uncertainties and its simplicity of implementation. It controls the output of the DC/DC boost converter by optimizing the recovery of photovoltaic power, particularly in fluctuating environmental conditions. The functional diagram presented in Figure 8 illustrates the interaction between the photovoltaic array, the converter and the fuzzy logic controller, demonstrating the effectiveness of the proposed architecture for dynamic tracking of the maximum power point.

Edelweiss Applied Science and Technology
ISSN: 2576-8484
Vol. 9, No. 7: 1748-1784, 2025
DOI: 10.55214/2576-8484.v9i7.9008

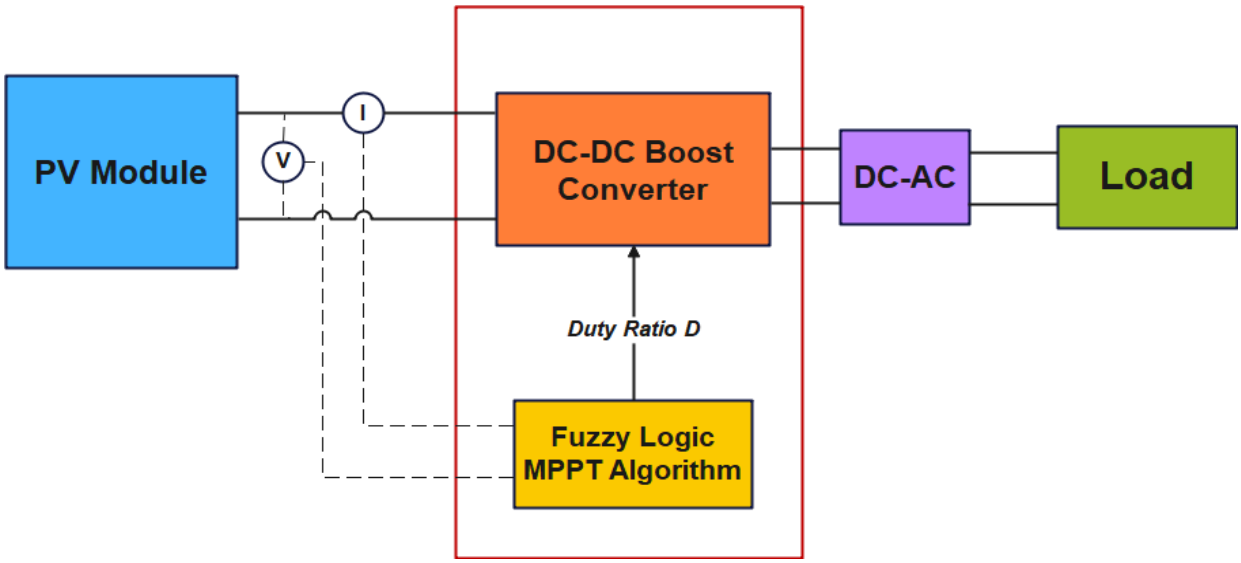

Figure 8.
Schematic diagram of the photovoltaic system and MPPT/FLC controller.

In the fuzzy logic MPPT algorithm, the voltage and current at each time k are detected to calculate the active power [47]. The active power is then compared with the power at the last time k-1 to obtain the power variation (ΔP(k)). Similarly, the current at time k is compared with the current at time k-1 to obtain the current error (ΔI(k)). Then, the power error is divided by the current error to obtain the error (E), which is compared with the previous error to calculate the error variation (ΔE(k)) as in equations (15) and (16), respectively. In this way, the error E(k) and ΔE(k) become the accurate inputs to the fuzzy logic controllers. The flowchart of the fuzzy logic MPPT is shown in Figure 9.

Edelweiss Applied Science and Technology
ISSN: 2576-8484
Vol. 9, No. 7: 1748-1784, 2025
DOI: 10.55214/2576-8484.v9i7.9008

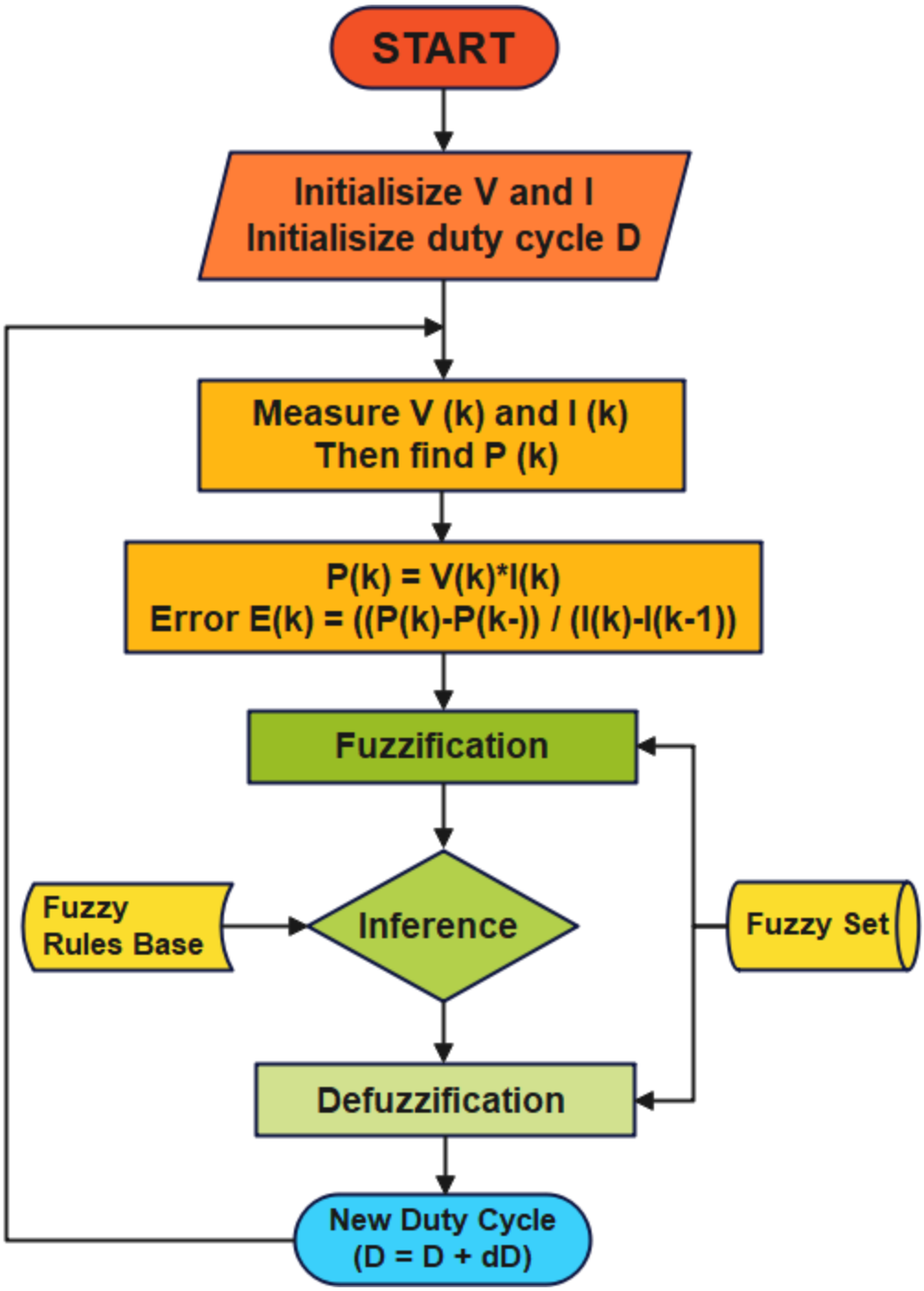

Figure 9.
Fuzzy logic maximum power point tracking (MPPT) flowchart.

In this work, Mamdani inference technique, A-type membership functions and 25-element rule base were used for fuzzy logic control. This technique is efficient and simple to define fuzzy output sets, and is more popular among researchers than other inference techniques [28]. The A-type, or triangular, membership function is used because it has less complexity when dividing values (low, medium and

Edelweiss Applied Science and Technology
ISSN: 2576-8484
Vol. 9, No. 7: 1748-1784, 2025
DOI: 10.55214/2576-8484.v9i7.9008

high) than other membership functions. Moreover, it has been observed that triangular membership function gives faster response and less overshoot than others. The 25-element rule base was used because it provides good performance [30, 46]. E and ΔE are represented respectively by equations (15) and (16):

$$E(k) = \frac{\Delta P(k)}{\Delta I(k)} = \frac{P(k) - P(k-1)}{I(k) - I(k-1)} \quad (15)$$

$$\Delta E(k) = E(k) - E(k-1) \quad (16)$$

Typically, a fuzzy logic controller consists of three components: (i) the fuzzifier , (ii) the inference, and (iii) the defuzzifier [48]. Each component is described individually below.

- *Fuzzifier:* This component of the fuzzy logic controller receives the input data and analyzes it according to a user-defined table, called a membership function. The Fuzzifier receives the data in a non-linear form and assigns it a score from 0 to 1. Membership functions have different forms. These depend on the data type, but the most common are S, π, A, and Z [31]. The form "A" was used in this work for the fuzzification operation.
- *Interference:* The inference system consists of a fuzzy rule which plays an important role in representing expert control or modeling knowledge between input and output. In the literature, different techniques are used in the inference system. Mamdani inference technique with fuzzy rule is employed in this work. The "if-then-else" statements are used in the system for fuzzy inference [49]. For example, a simple controller with two inputs and one output is considered, which has three fuzzy rules.

  Rule (1) IF X is A_2 OR Y is B1 Then Z is C_1
  Rule (2) IF X is A_2 AND Y is B2 Then Z is C_2
  Rule (3) IF X is A_1 Then Z is C_3

  Table 3 shows the fuzzy rules used to determine the desired MPP of the push-pull PWM converter.

Table 1.
Fuzzy logic rules for push pull converter. Negative Big (NB), Negative Small (NS), Zero (ZE), Positive Small (PS), Positive Big (PB).

Input		***ΔE (Change in error)***				
		NB	**NS**	**ZE**	**PS**	**PB**
E	NB	ZE	ZE	NB	NB	NB
	NS	ZE	ZE	NS	NS	NS
	ZE	NS	ZE	ZE	ZE	PS
	PS	PS	PS	PS	ZE	ZE
	PB	PB	PB	PB	ZE	ZE

- *Defuzzification:* In defuzzification, fuzzy logic controllers use the fuzzy rules to obtain the output value. This value depends on the defuzzification method. So, it is the value obtained by a fuzzy logic controller with respect to the label value in the fuzzy logic membership function. Seven fuzzy membership functions were used in this research, as shown in Table 3. These five functions are: Negative Big (NB), Negative Small (NS), Zero (ZE), Positive Small (PS), Positive Big (PB). In defuzzification, the FLC converts the fuzzy logic value into a data value. Many methods are available for the defuzzification process, such as the average weight (AW), center of gravity (COG), average of maximum (AOM), and smallest of maximum (SOM) method [50]. The COG method is used for MPPT, where all the fuzzy values converge to a single point. Fuzzy logic rules are used in the design of the boost-pull converter for MPPT, shown in Table 3 [49]. ΔD is calculated point by point by:

Edelweiss Applied Science and Technology
ISSN: 2576-8484
Vol. 9, No. 7: 1748-1784, 2025
DOI: 10.55214/2576-8484.v9i7.9008

$$\Delta D = \frac{\sum_{J=1}^{n} \mu\left(\Delta D_j\right).\Delta D_j}{\sum_{J=1}^{n} \mu\left(\Delta D_j\right)} \quad (17$$

$$D(k) = D(k-1) + S_{\Delta D}.\Delta D(k) \quad (18$$

2.3. Battery Energy Storage Model

The simulations under Matlab/Simulink were calibrated using experimental data from recognized resources in Li-ion battery modelling [51, 52] thus ensuring adequacy with the real dynamics of the system. The battery model incorporates aging parameters, based on previous studies, in order to reflect operational constraints in tropical environments, particularly with regard to charge/discharge cycles at high rates.

Batteries, as energy storage devices, are key components of microgrids due to their ability to store energy in the form of electrochemical potential from various energy sources for later use. Their role in energy management within hybrid systems is fundamental, particularly in balancing production and demand. The charging and discharging of stored energy depends on the difference between the power produced by renewable sources ($PG_{Renewable,t}$), calculated according to equation (19), and the load demand ($PL_{Demand,t}$).

Matlab/Simulink simulations were calibrated using experimental data from recognized resources in Li-ion battery modeling, ensuring adequacy with real-world dynamics. The battery model incorporates aging parameters based on previous studies, reflecting operational constraints in tropical environments.

Batteries are among the most efficient energy storage devices. They can store energy in the form of electrochemical potential and from various energy sources for later use. They are essential as fundamental components of microgrids [53]. The charging and discharging of the energy stored in the battery bank depends on the difference between the power produced by renewable sources ($PG_{Renewable,t}$) calculated by equation (19) and the consumed load demand ($PL_{Demand,t}$).

$$PG_{Renewable,t} = PG_{Pv,t} + PG_{Wt,t} \quad (19)$$

The evolution of the state of charge (SOC) of the accumulator at each instant t is determined by coulometry. During charging, it is calculated by equation (20) as follows:

$$SOC(t) = SOC(t-\Delta t) + (PG_{Pv,t} \times \eta_{dcdc} + PG_{Wt,t} \times \eta_{acdc} - \frac{PL_{Demand,t}}{\eta_{wr} \times \eta_{inv}}) \times \frac{\eta_{cha}}{U_{bus}} \times \Delta t \quad (20)$$

In the discharge phase, the state of charge is given by equation (21):

$$SOC(t) = SOC(t-\Delta t) + (PG_{Pv,t} \times \eta_{dcdc} + PG_{Wt,t} \times \eta_{acdc} - \frac{PL_{Demand,t}}{\eta_{wr} \times \eta_{inv}}) \times \frac{1}{\eta_{dis} \times U_{bus}} \times \Delta t \quad (21)$$

$PL_{Demand,t}$ is the power consumed by the residential dwelling at time t. Δt is the simulation step. It is half an hour. η_{dcdc}, η_{acdc} and η_{inv} are the respective efficiencies of the DC/DC, AC/DC and DC/AC converters (Figure 10). They are all equal to 0.95 [45]. η_{cha} and η_{dis} are the charge and discharge efficiencies of the batteries. Although debatable, the values in the literature [54, 55] ($\eta_{cha} = 0.85$, $\eta_{dis} = 1$) have been retained. η_{wr} is introduced to take into account losses in cables and connections ($\eta_{wr} = 0.98$ [54]). U_{bus} is the nominal voltage of the DC bus. It is chosen at 48 V. This is a standard value that meets safety conditions.

Edelweiss Applied Science and Technology
ISSN: 2576-8484
Vol. 9, No. 7: 1748-1784, 2025
DOI: 10.55214/2576-8484.v9i7.9008

In order to control the lifetime of batteries, their state of charge (SOC) is subject to the constraints of the following equation (22):

$$SOS_{min} \leq SOC(t) \leq SOS_{max} \quad (22)$$

SOC_{max} and SOC_{min} being the maximum and minimum storage capacities allowed. SOC_{max} corresponds to the nominal capacity of the assembled accumulators C_n in equation (23):

$$C_n = \left(\frac{N_{bat}}{N_{bats}}\right) \times C_{bat} = N_{batp} \times C_{bat} \quad (23)$$

Where: C_{bat}: capacity of an elementary battery; N_{bat}: total number of batteries; N_{bats}: total number of batteries connected in series in each branch. Equation (24) shows how to calculate this number from the DC bus voltage U_{bus} and the nominal voltage of each battery V_{bat} (here 12 V):

$$N_{bats} = \frac{U_{bus}}{V_{bat}} = \frac{48}{12} = 4 \quad (24)$$

The SOC_{min} corresponds to the lower limit that the storage bench must not exceed during discharge. It is determined by equation (25) as follows:

$$SOS_{min} = (1 - DOD_{max}) \times SOS_{max} \quad (25)$$

DOD_{max} is the maximum depth of discharge (DOD) that batteries can accept. It depends on the battery type and the application. In the case of stand-alone energy systems in isolated locations, most batteries used are deep-cycle lead-acid batteries (VRLA technology is now widely used) [56]. A discharge depth of 70% is tolerated [54].

The battery storage system is connected to the DC/DC converter, and then its output is connected to a common constant voltage DC bus. All energy transfer, whether from sources to battery, from sources to load, or from storage system to load, is done through this constant voltage DC bus. Since the energy flow associated with the battery is not unidirectional, a bidirectional converter is required to charge and/or discharge the battery in case of excess and/or deficit energy, as shown in Figure 10.

Edelweiss Applied Science and Technology
ISSN: 2576-8484
Vol. 9, No. 7: 1748-1784, 2025
DOI: 10.55214/2576-8484.v9i7.9008

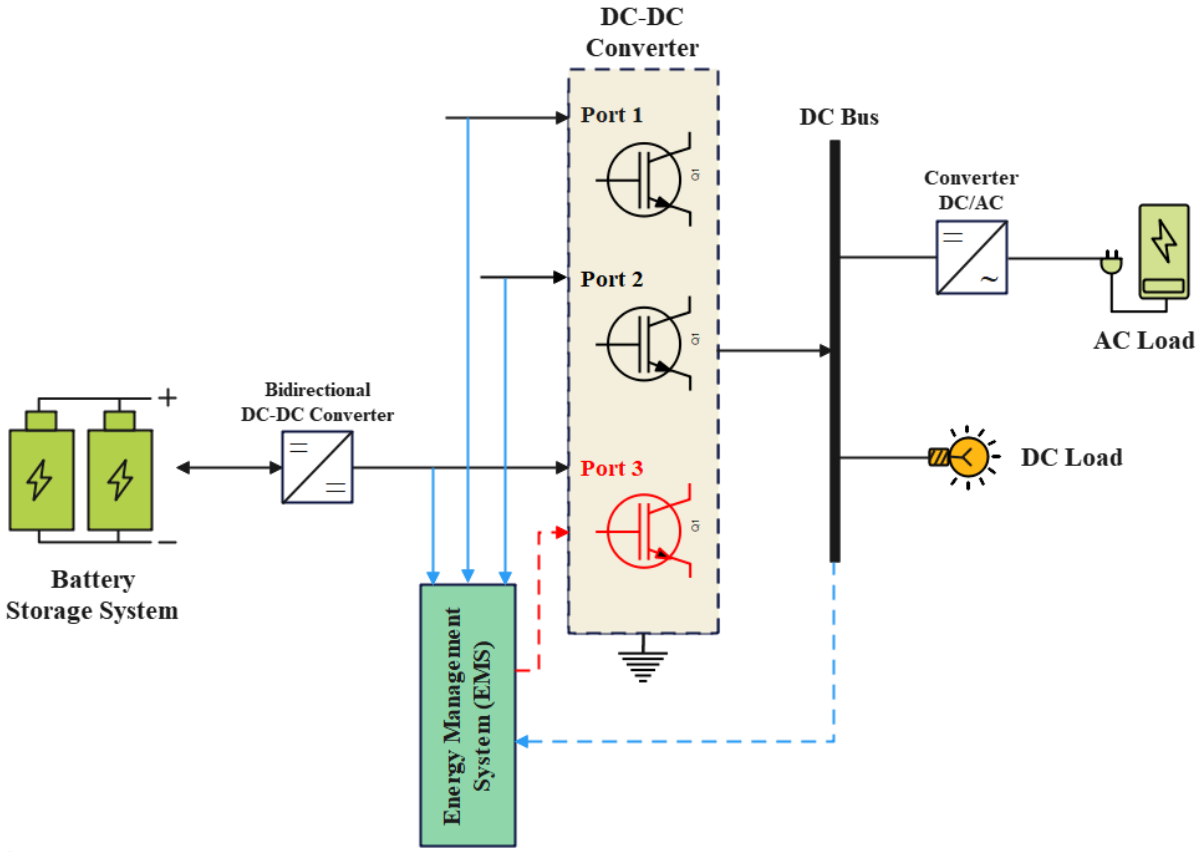

Figure 10.
The battery storage system.

The controller parameters are used to regulate the power flow from both sources and the load demand. The variable component of the structure is the error ΔP, calculated using the following equation (26):

$$Error(\Delta P) = PG_{Renewable,t} - PL_{Demand,t} \quad (26)$$

When the P performance Δis actual, the control system is charging; when it is lower, it is discharging. Thus, the bidirectional DC/DC converter allows the energy flow to be managed in both directions, depending on the needs.

2.4. Energy Management System (EMS)

The Energy Management System (EMS) is the main controller that coordinates and controls all regulation actions of the hybrid system. All converter controllers presented in the previous sections operate in EMS control mode [57, 58]. The boost converter of the solar photovoltaic/wind energy conversion system operates in two modes, depending on the energy production: MPPT mode and non-MPPT mode [54].

The bidirectional battery converter operates in charge or discharge mode and keeps the DC bus voltage constant. The DC/AC boost converter of the wind energy conversion system operates in boost mode [55]. The power of the microgrid needs to be balanced under different conditions of renewable energy generation and load demand. The power balance equation (27) of the hybrid system is as follows:

$$PG_{Renewable,t} = PL_{Demand,t} + P_{Bat} \quad (27)$$

Edelweiss Applied Science and Technology
ISSN: 2576-8484
Vol. 9, No. 7: 1748-1784, 2025
DOI: 10.55214/2576-8484.v9i7.9008

2.5. Dynamic Simulation of Hybrid System

To simulate the hybrid PV/wind system with storage, a dynamic model under Matlab/Simulink was used. The modeling process of the Simulink model of the hybrid system is as follows: (i) Simulation of the PV model in Simulink; (ii) Simulation and observation of the wind turbine performance; (iii) Modeling and simulation of the charging and discharging capacities of the battery bank; (iv) Use of the hybrid renewable energy system (HRES) to supply electricity to the building loads. The operating principle of the developed simulator can be summarized by the timing diagram in Figure 11.

Edelweiss Applied Science and Technology
ISSN: 2576-8484
Vol. 9, No. 7: 1748-1784, 2025
DOI: 10.55214/2576-8484.v9i7.9008

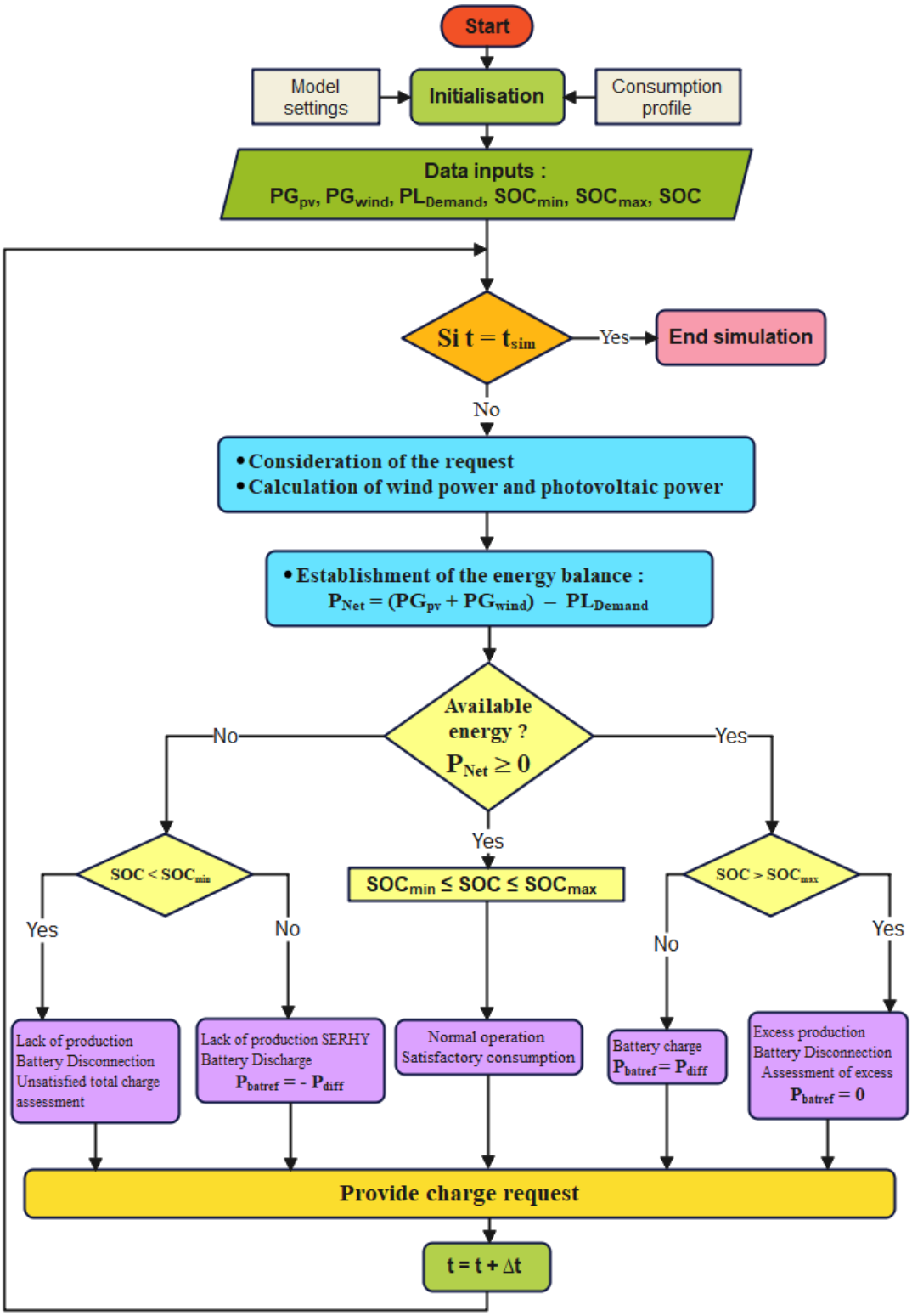

Figure 11.
Synoptic simulation of the operation of a system.

Edelweiss Applied Science and Technology
ISSN: 2576-8484
Vol. 9, No. 7: 1748-1784, 2025
DOI: 10.55214/2576-8484.v9i7.9008

The first phase is an initialization phase where the original parameters of the system are fixed (component size and initial state of charge of the batteries). Given the duration considered for the simulations, we can consider that the initial state of charge of the batteries has no impact on the results. Then, the same loop will be repeated for each time step of the simulation (Δt) until the simulation time (t_{sim}) is reached.

For a given system configuration, after taking into account the consumer's electrical demand $PL_{Demand,t}$, the total power produced by the wind and photovoltaic generators $PG_{Renewable,t}$ is evaluated at each calculation step Δt, the losses in the converters (MPPT PV chopper, wind turbine AC/DC converter and inverter) and in the cables are deducted. The charging and discharging of the batteries can then be controlled by the difference between the production injected on the DC bus (production reduced by the converter losses) P_{Res} and the consumer's demand on the DC bus (demand increased by the inverter losses and in the cables) $PL_{Demand,t}$. A switcher ensures energy management according to different scenarios:

- *Normal operation*, during which the consumer is fully satisfied and the state of charge at $t + \Delta t$ is within the minimum and maximum thresholds imposed to ensure proper operation of the accumulator. The batteries are connected and two cases can occur:
- If the state of charge of the accumulators is lower than SOC_{max} (set at 100%) and $PL_{Demand,t} < P_{Res}$, then the excess production $(P_{Res} - PL_{Demand,t}).\Delta t$ is stored in the batteries.
- If the battery state of charge is greater than SOC_{min} (set at 30%) and $PL_{Demand,t} > P_{Res}$, then in this case the previously stored energy is used to compensate for the lack of production $(PL_{Demand,t} - P_{Res}).\Delta t$.
- *Degraded operation*, during which the estimated state of charge exceeds one of the imposed thresholds. In this case, the switcher is opened and the batteries are disconnected. Two scenarios are possible:
- Lack of production: it occurs when there is an overconsumption ($PL_{Demand,t} > P_{Res}$) associated with a state of charge at $t + \Delta t$ calculated lower than the minimum threshold of the accumulator. This means that the SOC min threshold is reached. In the case where the consumer is equipped with a home automation system allowing certain loads to be individually shed (the least common case), the consumer's electrical demand must therefore be shed (partial consumption shed mode). We then speak of a shortage of capacity or unsatisfied demand. This lack of production can be evaluated for the shed period Δt as $(PL_{Demand,t} - P_{Res}).\Delta t$.
- Excess production: it occurs in the case of an overproduction ($P_{Res} > PL_{Demand,t}$) accompanied by a calculated state of charge higher than the maximum threshold allowed for the accumulator. This excess can be quantified for its duration Δt as $(P_{Res} - PL_{Demand,t}).\Delta t$.

3. Results and Discussions

This section presents the performance results of the autonomous hybrid system, aiming to efficiently manage load variations and external disturbances while maintaining optimal stability of the wind and photovoltaic system. The simulations carried out allow the evaluation of the energy efficiency and stability of the system under different operating scenarios. The collected data were analyzed using robust statistical methods, allowing the identification of significant trends and relevant correlations. The results highlight the Simulink models, thus offering new perspectives on the individual and combined contributions of renewable energy sources, highlighting their complementarity. The study then focuses on the management and behavior of the battery to ensure the balance between energy production and consumption.

Finally, the results obtained will be compared to alternative configurations or similar work, in order to better situate the performance of our system and identify possible areas for improvement.

Edelweiss Applied Science and Technology
ISSN: 2576-8484
Vol. 9, No. 7: 1748-1784, 2025
DOI: 10.55214/2576-8484.v9i7.9008

Simulations performed in MATLAB allow us to evaluate the management and operation of the modeled wind system. The results obtained highlight the dynamic behavior of the wind turbine as a function of wind variations and load conditions. Figure 12 below represents the Simulink model of a wind system designed in Simulink. The wind model provides three input data to the system: generator speed, tilt angle, and wind speed.

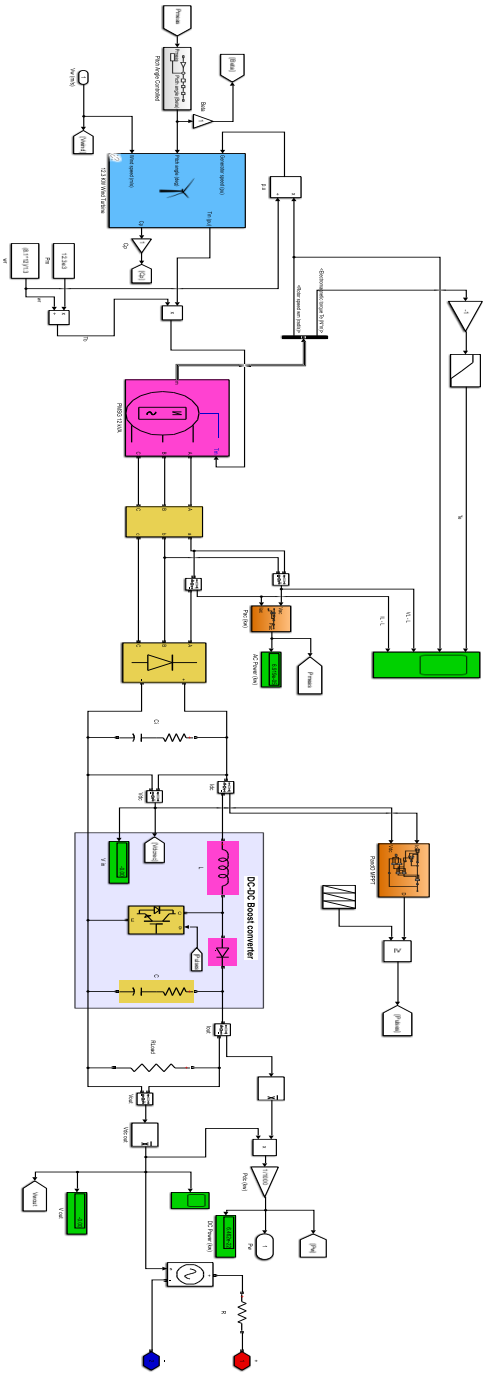

Figure 12.
Simulink model of the wind energy system.

Edelweiss Applied Science and Technology
ISSN: 2576-8484
Vol. 9, No. 7: 1748-1784, 2025
DOI: 10.55214/2576-8484.v9i7.9008

A mathematical model of a photovoltaic panel, including the fundamental components (diode, current source, series resistance, and parallel resistance), is studied with tags and modeled in the Simulink environment. The simulation of the solar module was carried out using the equations presented in the previous section and then followed sequentially. The ideal characteristics of a photovoltaic field are verified under standard test conditions. Similar conditions are designed in Simulink, a Matlab programming language for simulating and analyzing multi-domain functions or systems. The complete subsystem of the photovoltaic cell is obtained as shown in Figure 13 below:

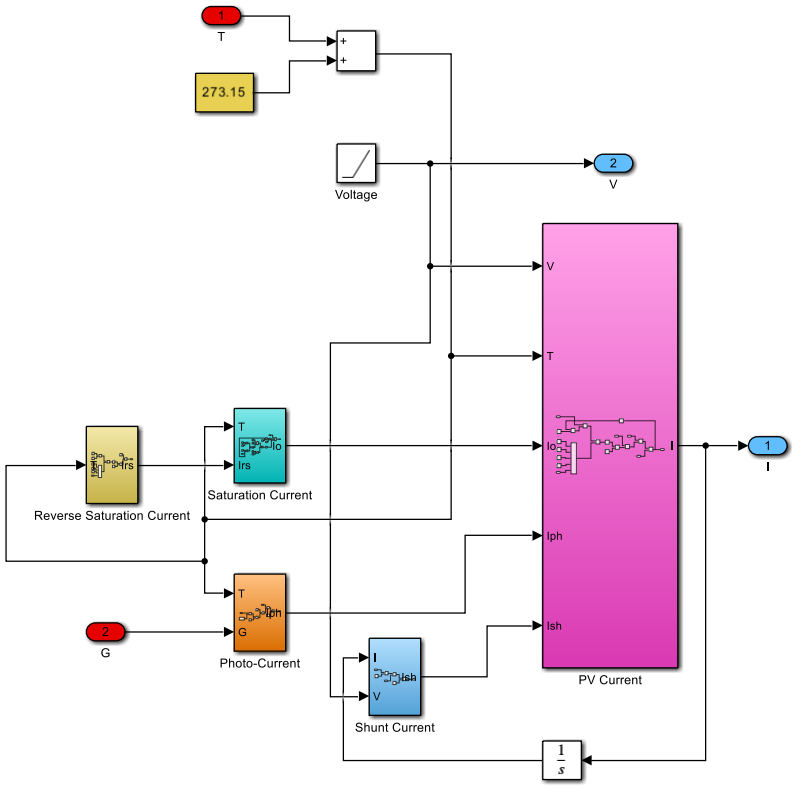

Figure 13.
Complete PV subsystem.

He whole PV system, converter and MPPT controller is shown in Figure 14 below: the PV array model is connected to the DC/DC boost converter, it was developed for extracting the maximum power from the PV panel.

Edelweiss Applied Science and Technology
ISSN: 2576-8484
Vol. 9, No. 7: 1748-1784, 2025
DOI: 10.55214/2576-8484.v9i7.9008

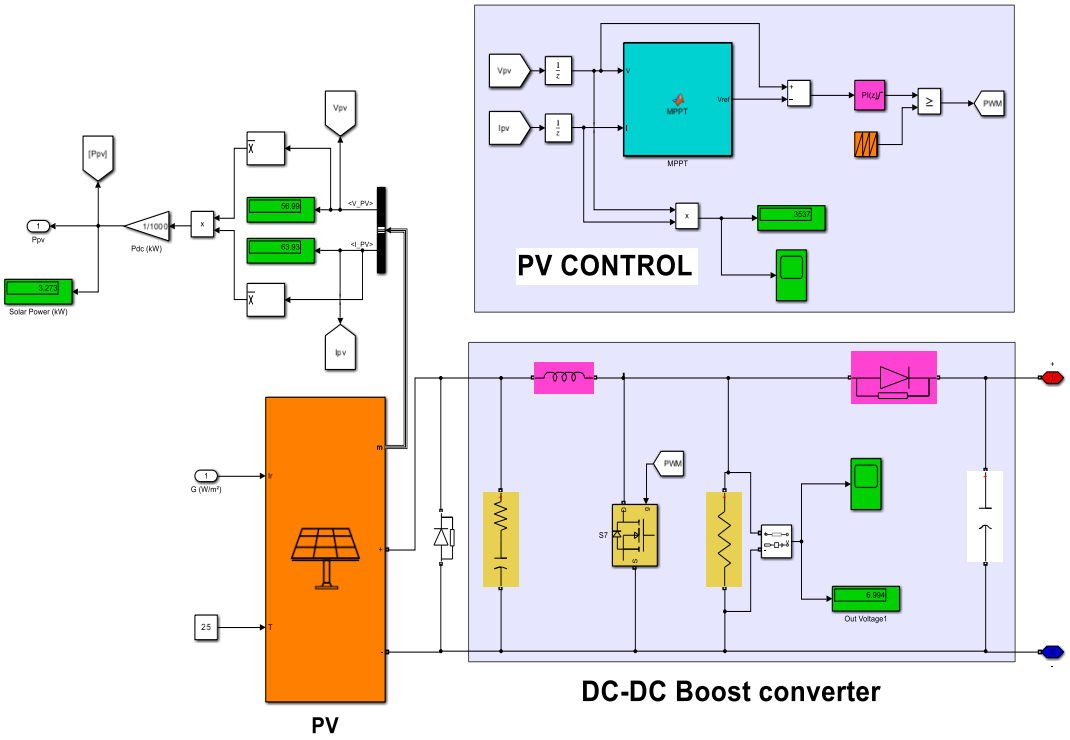

Figure 14.
The Simulink model of the photovoltaic generator.

To this DC/DC boost converter, an MPPT controller based on the FLC fuzzy rules was added, whose membership functions are shown in Figure 14. Each membership degree has five basic fuzzy subsets for the input variables, shown in Figure 15.a and Figure 15.b, and five fuzzy subsets for the output variables, shown in Figure 15.c. The parameterization of the fuzzy controller rules was defined and Figure 16 illustrates the three-dimensional fuzzy map of the fuzzy logic controller for PV system power optimization.

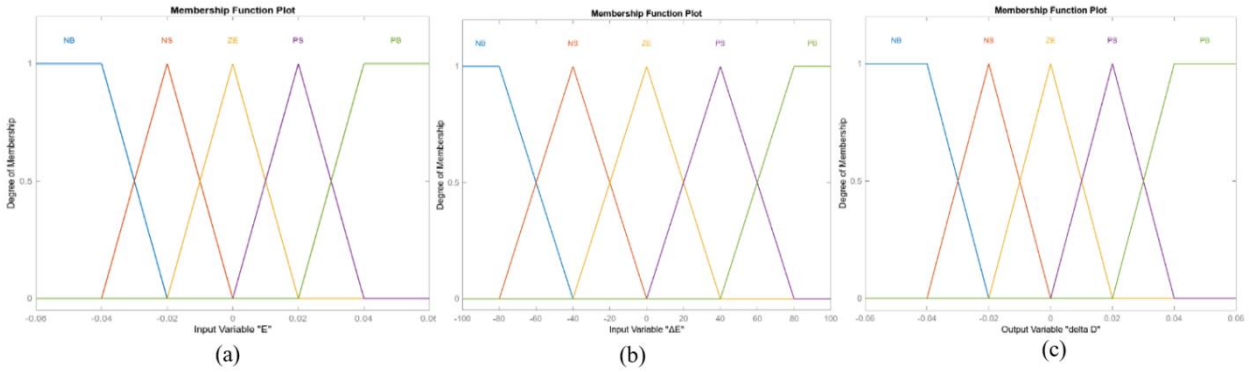

Figure 15.
Fonctions d'appartenance utilisées dans le contrôleur flou : (a) erreur E, (b) variation de l'erreur ΔE, (c) variation du facteur de commande ΔD.

Edelweiss Applied Science and Technology
ISSN: 2576-8484
Vol. 9, No. 7: 1748-1784, 2025
DOI: 10.55214/2576-8484.v9i7.9008

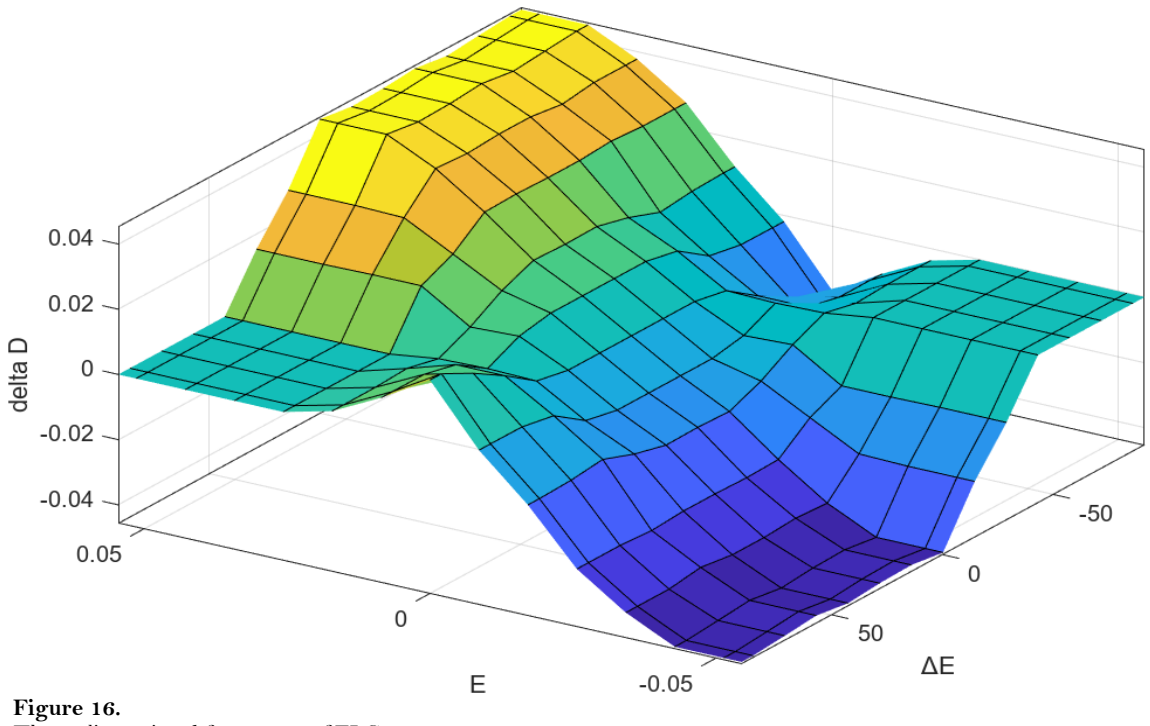

Figure 16.
Three-dimensional fuzzy map of FLC.

The FLC-based MPPT system was integrated into the boost converter for power tracking. The results of the proposed model were compared with those of the conventional P&O MPPT method. The simulation results show that this method effectively tracks the maximum power point under uncertain conditions. It also reduces oscillations around the maximum power point and provides a better response than the conventional P&O method. Comparison of the maximum power tracking efficiency in the photovoltaic module reveals that the proposed method is more efficient than other P&O-based MPPT methods.

Figure 17 and Figure 18 illustrate the Simulink model of the storage system with its charge/discharge controller. This controller is designed to manage the energy flows into and out of the battery. Thus, in case of excess energy (i.e., when supply is greater than demand), the battery charges, allowing the converter to operate directly. In case of power deficit (i.e., when supply is less than demand), the battery starts discharging, supplying the deficit to the load.

Edelweiss Applied Science and Technology
ISSN: 2576-8484
Vol. 9, No. 7: 1748-1784, 2025
DOI: 10.55214/2576-8484.v9i7.9008

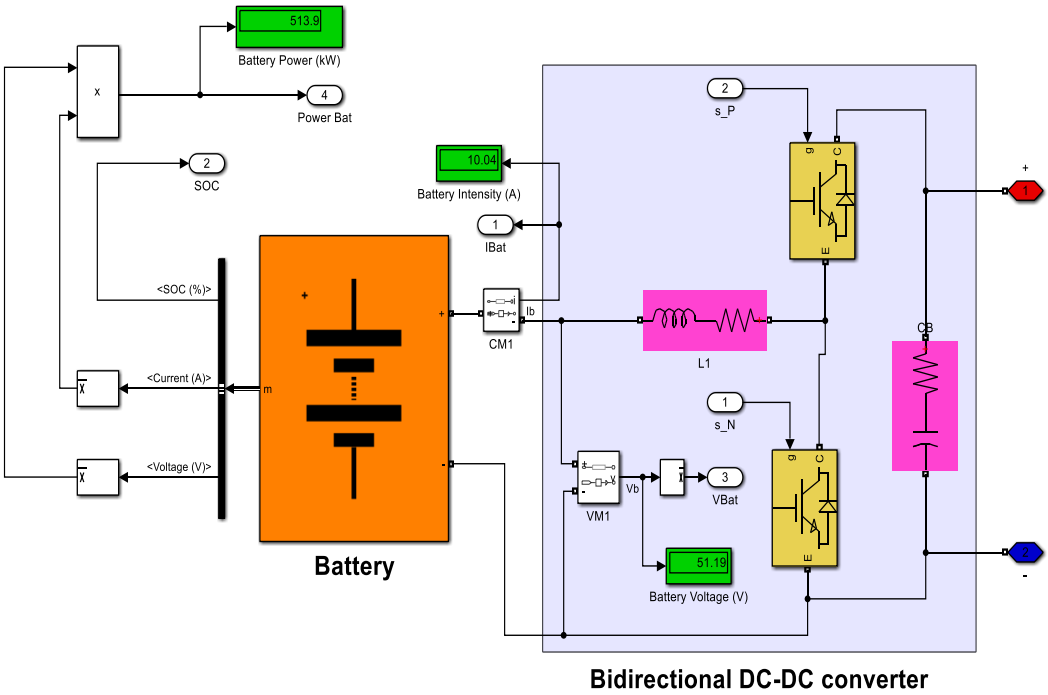

Figure 17.
Simulink model of bidirectional DC/DC converter.

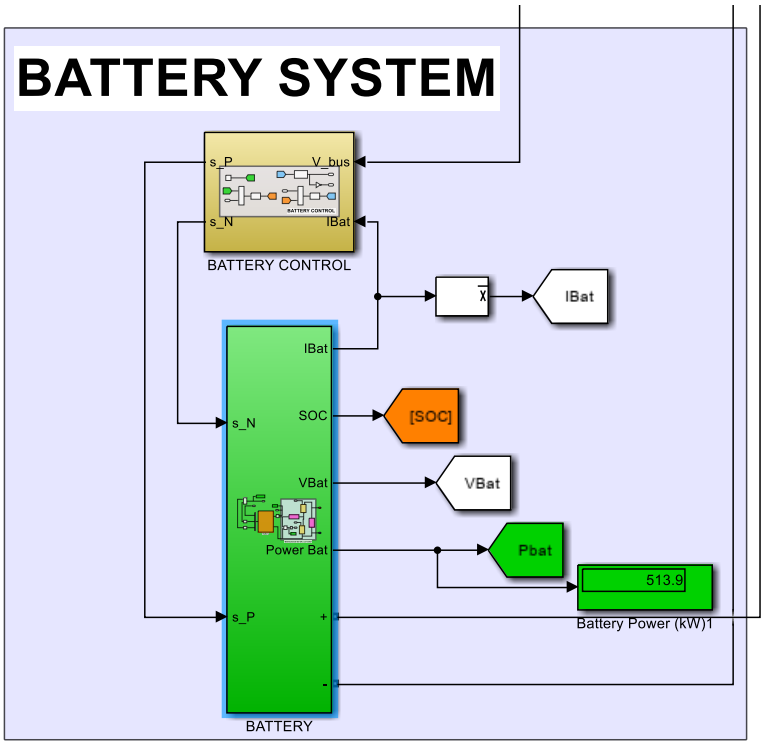

Figure 18.
Simulink battery model and charge-discharge controller.

Edelweiss Applied Science and Technology
ISSN: 2576-8484
Vol. 9, No. 7: 1748-1784, 2025
DOI: 10.55214/2576-8484.v9i7.9008

The determination of the control scheme remains evaluated in this research using MATLAB/Simulink. In order to demonstrate the robustness of the hybrid energy system, three main conditions are modeled. The schematic illustration of the load mix organization is shown in Figure 19 and presents the developed simulator. It consists of a wind turbine model, a photovoltaic generator model, an ideal battery model and an energy management and load regulation subsystem. This subsystem allows stopping the charging process when the storage bank capacity reaches its maximum value (SOC_{max}).

In this case, if the total power produced by the photovoltaic generator and the wind turbine is greater than the power demanded by the consumer (all losses combined), an excess of energy is recorded. Otherwise, if the battery capacity reaches its minimum level (SOC_{min}), some devices are discharged. Consequently, the household's electricity needs are not met. We then consider an insufficiency of the power produced by the hybrid system.

Edelweiss Applied Science and Technology
ISSN: 2576-8484
Vol. 9, No. 7: 1748-1784, 2025
DOI: 10.55214/2576-8484.v9i7.9008

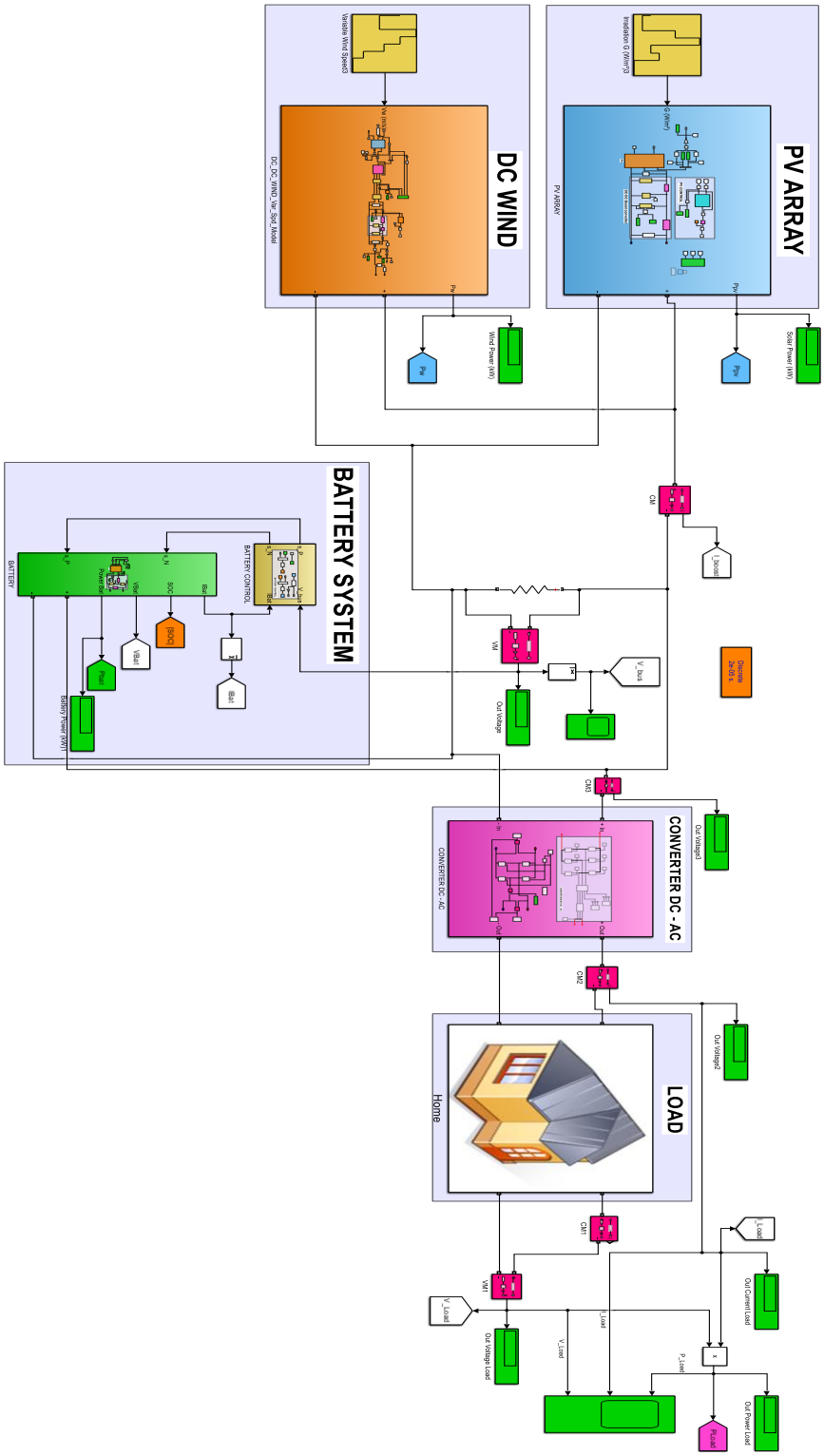

Figure 19.
Simulink modeling of the wind-photovoltaic hybrid system with batteries.

Edelweiss Applied Science and Technology
ISSN: 2576-8484
Vol. 9, No. 7: 1748-1784, 2025
DOI: 10.55214/2576-8484.v9i7.9008

The hybrid production management system with the different loads is developed using the timeline in Figure 11. The renewable energy blocks used are photovoltaic, wind turbine and battery to store the produced energy. Different relays or switches allow to activate or deactivate a connection according to the user's needs, while optimizing comfort and safety. Figure 20 shows the state-flow diagram under the Matlab/Simulink environment which groups the different blocks.

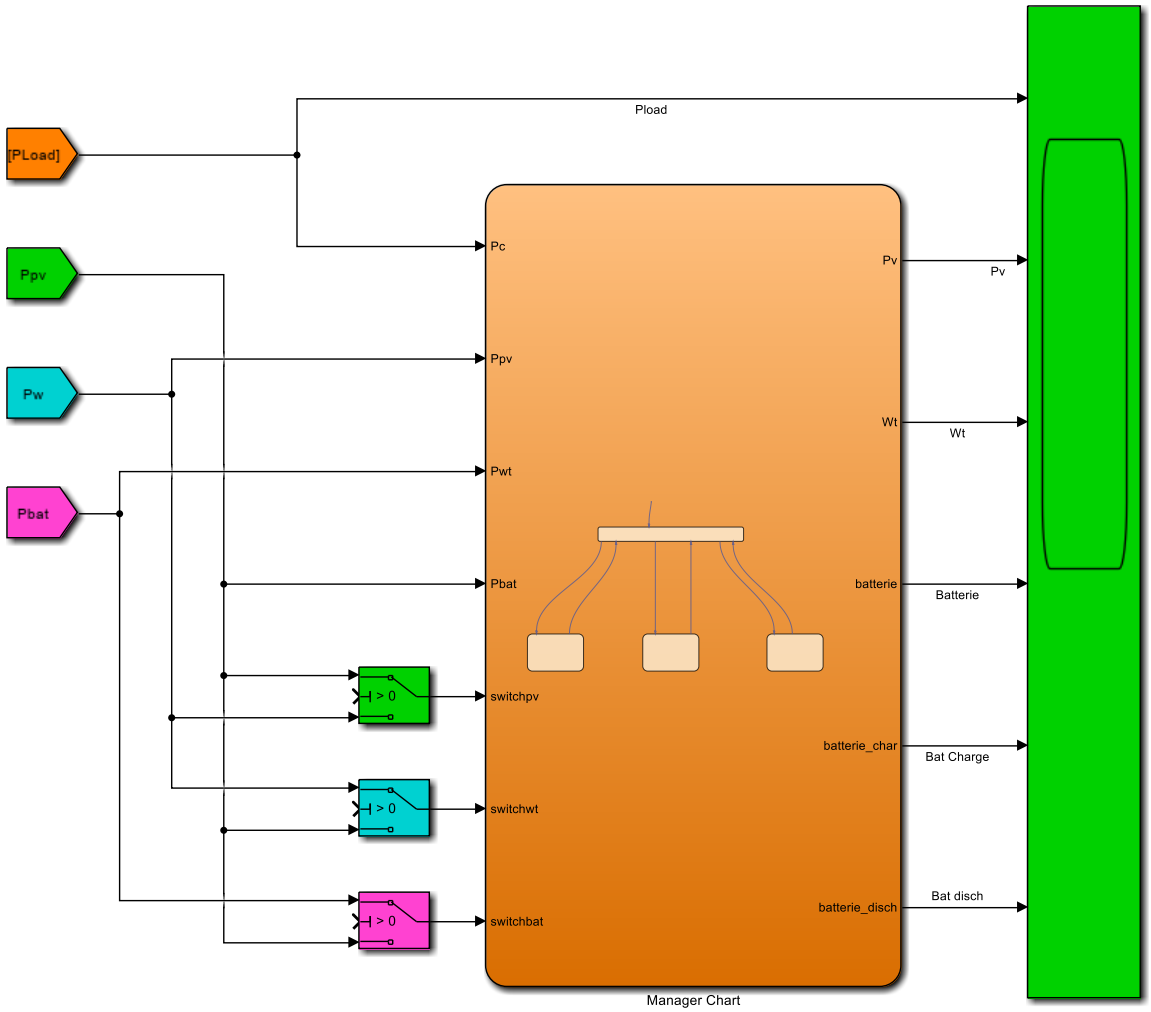

Figure 20.
The energy management model under Matlab/Simulink.

He scenarios in Table 4 are defined based on the weather conditions favorable to the operation of each source. This will be activated or deactivated to efficiently meet the load needs in real time. The battery comes into operation to meet the demand in case of unavailability of both sources. Solar radiation varies from 0 to 1000 W/m², but is in the intermediate category to be raised. The temperature is typically 25 °C and the wind speed varies from 0 to 12 m/s.

Edelweiss Applied Science and Technology
ISSN: 2576-8484
Vol. 9, No. 7: 1748-1784, 2025
DOI: 10.55214/2576-8484.v9i7.9008

Table 4.
Scenarios according to the energy supply and demand of the hybrid system.

Load	PV				Wind				Battery	
kW	W/m²	I(A)	V(V)	P(W)	Speed	I(A)	V(V)	P(W)	(A)	P(W)
30	1000	69.17	761.6	5.27E+04	12	8.58	615.96	5274.53	0	7616
30	500	33.57	735.1	2.47E+04	8	9.08	615.25	5584.14	-5	-3676
30	250	15.97	715.2	1.14E+04	4	7.13	614.25	4381.5	-15	-1.07e+4
30	0	0	705.1	0	0	2.57	614.3	1580.19	-25	-1.76e+4
40	1000	69.17	750.1	5.19E+04	12	19.57	615.65	8500	10	7501
40	500	33.57	716.3	2.41E+04	8	10.17	614.8	6254.52	155	-1.07e+4
40	250	15.97	705.1	1.13E+04	4	5.53	614.26	3398.46	-25	-1.76e+4
40	0	69.17	761.6	5.27E+04	0	0.56	613.65	343.37	-25	-1.72e+4

Figure 21 shows the simulation connection diagram of a solar-wind microgrid. The objective of the first case is to provide constant power to the load under different production conditions. The sunshine varies by turning the lamps on and off, resulting in different levels of sunshine. Although variations in wind speed and sunshine are only gradual variations, they can never occur in real-life situations, as weather conditions are constantly changing. Moreover, in this case, the load is kept constant, which would not be the case in practice.

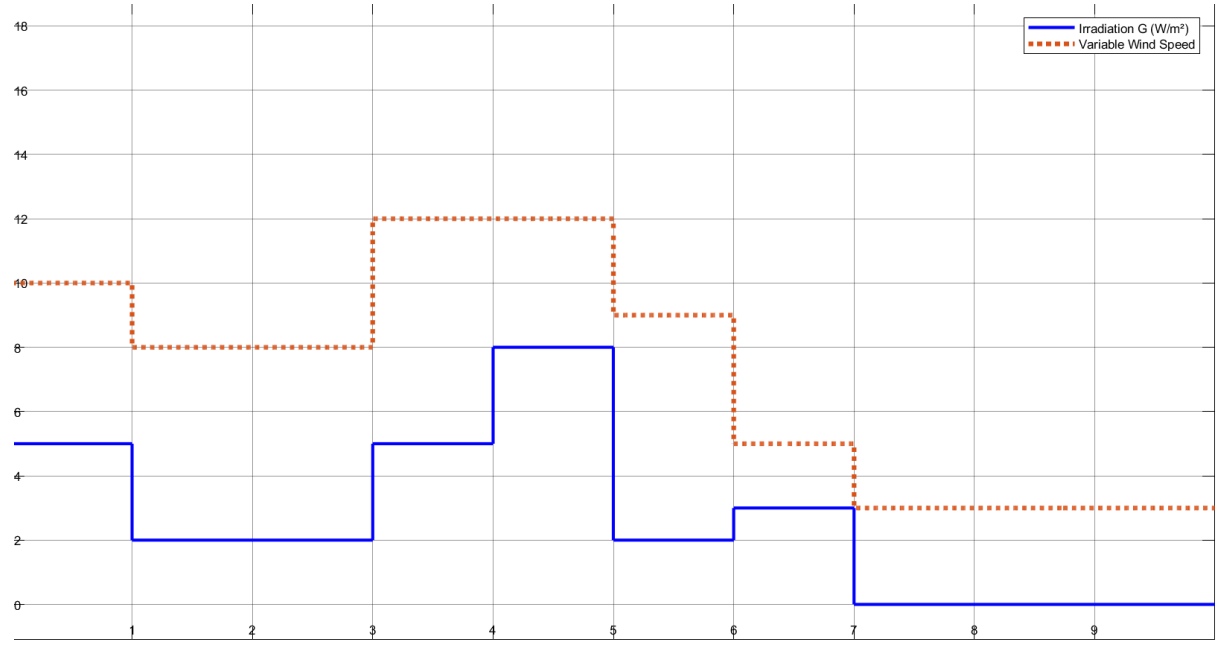

Figure 21.
Solar irradiance and wind speed as a function of time.

These values are chosen such that they vary between the maximum and minimum possible operating range of the PV panel and the wind turbine in order to verify the operation of the system for these variations, as shown in Figure 21.

In this study, the simulation results of the wind-photovoltaic hybrid system were presented, integrating various performance metrics such as voltage, current, load voltage, as well as the active power of the generators and the battery power. Figure 22 to Figure 25 illustrate these results by detailing the voltage, current and load voltage of the two generators, the load level and the battery power. They also provide information on the overall voltage of the hybrid system, as well as the current of the load and the storage system. At different times, the activation of the hybrid system results in the

intervention of the filter current in order to compensate for the harmonic currents generated by the load.

The simulations take into account the temporal evolution of energy production, taking into account variations in sunlight and wind speed. The following figures present this evolution, allowing the performance of each energy source to be evaluated according to varying environmental conditions.

Figure 22 illustrates the simulation results of the photovoltaic production in the studied hybrid system, highlighting a strong linear correlation between the irradiance (200 - 1000 W/m²) and the output power, with a determination coefficient of $R^2 = 0.98$, reflecting the accuracy of the model. The overall system efficiency reaches 15.2% at 25 °C , which is in line with the performance ranges typically observed in the literature [39]. The thermal impact is also taken into account: an ambient temperature increase of +10 °C results in an efficiency decrease of about 0.45%/°C, in accordance with equation (13), and in agreement with the derating coefficients reported in previous studies.

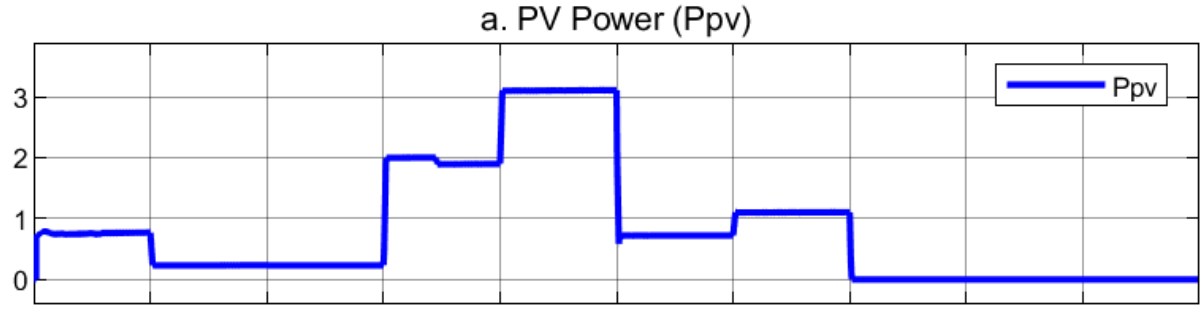

Figure 22.
Temporal variation of photovoltaic (PV) energy production.

The simulations performed in MATLAB/Simulink allow a dynamic evaluation of the PV system behavior in the face of environmental variations (sunshine, temperature), with a set frequency stabilized at 50 Hz. Although the load demand remains constant, the output power of the solar field varies according to the irradiation, reaching 1.5 kW under nominal conditions. Thanks to the fuzzy logic MPPT controller, the extracted power is optimized to about 2 kW, translating a conversion efficiency close to 100% under the simulated conditions. This result is also visible on the time profiles, where the activation of the main transistor allows a dominant contribution of the PV to the grid, while the other components remain in standby.

The proposed fuzzy MPPT controller is distinguished by a fast response time of 0.4 s, largely outperforming conventional approaches such as P&O (1.8 s) and artificial neural networks (0.9 s), as reported in Table 5 and by Asif, et al. [31]. This fast behavior allows efficient system adaptation to rapid insolation variations, while reducing energy tracking losses.

Finally, the simulation results confirm the robustness of the model in the face of typical operating conditions in tropical environments. They also highlight several avenues for improvement, including the integration of passive or active thermal management solutions to limit losses due to module heating, as well as coupling with a storage system to smooth production and improve power supply stability.

Figure 23 illustrates the time evolution of the wind power output of the hybrid system, highlighting the non-linear relationship between wind speed (4 to 12 m/s) and the power extracted via the permanent magnet synchronous generator (PMSG). The coefficient of performance Cp reaches a maximum of 0.515 for an optimal speed ratio $\lambda = 7.2$, reflecting an efficient aerodynamic conversion in the simulated operating ranges.

The power curves confirm a response in line with theoretical expectations, with production stabilized around 5 kW after AC/DC conversion and a power peak reaching 6 kW thanks to the implementation of the fuzzy MPPT controller. The latter allows optimal extraction of the available

energy, despite variations in wind speed. The AC/DC inverter, in addition to regulating the supply voltage, ensures active smoothing of the injected current, limiting the total harmonic distortion (THD) to less than 3.2%, in accordance with the requirements of the IEC 61000-3-2 standard [59].

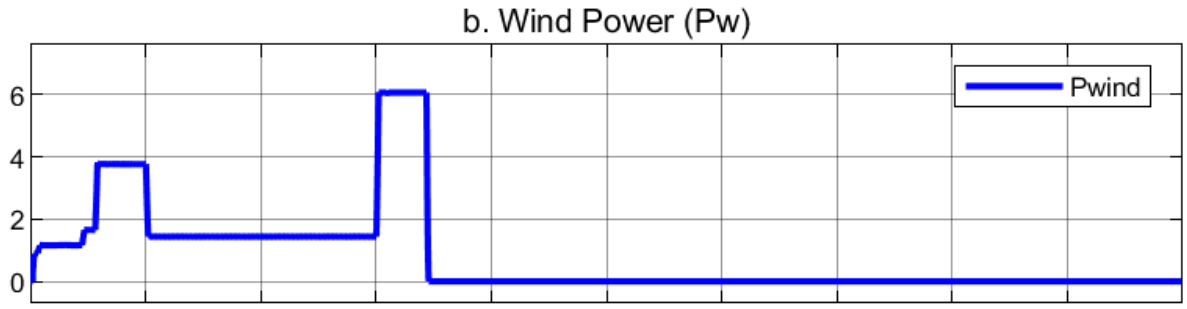

Figure 23.
Temporal fluctuation of wind power production.

The performance analysis shows that the power at the PMSG is highly dependent on wind fluctuations. However, the overall efficiency of the wind system, estimated between 85% and 100% according to the scenarios in Table 4, only concerns the post-PMSG electrical conversion. Mechanical losses and aerodynamic limitations upstream of the generator, particularly due to turbulence or extreme wind regimes, can affect the actual productivity of the turbine.

In extreme conditions (very low or high speeds), the system shows limitations that justify the integration of adaptive protection mechanisms or partial decoupling strategies to preserve the integrity of the components. Furthermore, in order to improve the resilience and overall efficiency of the hybrid architecture, solutions such as complementary energy storage, or the implementation of intelligent adaptive controllers are recommended to compensate for transient instabilities and smooth the power injected into the local network.

Figure 24 highlights the dynamic complementarity of photovoltaic and wind sources within the hybrid architecture. Simulations demonstrate a dominance of photovoltaic production during the daytime, reaching up to 73% of the total energy contribution at midday, while wind generation becomes predominant during the night hours, with a peak coverage of 62%. This inter-seasonal and inter-daily complementarity makes it possible to compensate for the intermittencies specific to each technology, ensuring continuity of energy supply.

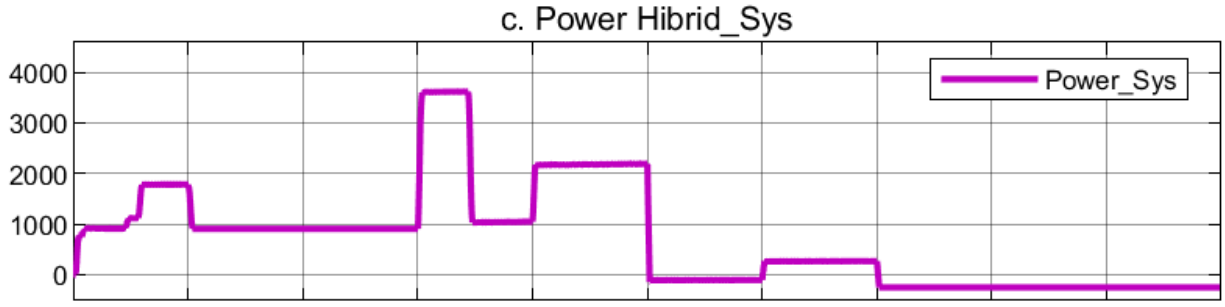

Figure 24.
Comparison of photovoltaic, wind and combined energy production.

The two sources were synchronized via DC/DC conversion buses, allowing efficient aggregation of the produced power and its stabilized injection into the distribution system. Thanks to the use of high-efficiency Boost converters, the power of the two generators could be optimized individually, before

Edelweiss Applied Science and Technology
ISSN: 2576-8484
Vol. 9, No. 7: 1748-1784, 2025
DOI: 10.55214/2576-8484.v9i7.9008

their coupling to the common DC bus. The system thus maintains a stable bus voltage of 48 V ± 1.5%, even during sudden variations in demand or production (ΔP = ±30%), demonstrating the robustness of the adopted energy management strategy.

Figure 25 illustrates the charge (t = 0 s and t = 5 s) and discharge (t = 5 s and t = 10 s) cycles of the battery storage system, ensuring energy balancing during the transient phases between production and consumption. The overall storage efficiency reaches a round-trip efficiency of 85%, decomposed into $\eta_{charge} = 0.85$ and $\eta_{discharge} = 0.98$, in accordance with the values observed in the literature [60]. This storage device plays a key role in voltage regulation, instantaneous power smoothing and security of supply in the event of a transient failure of a primary source.

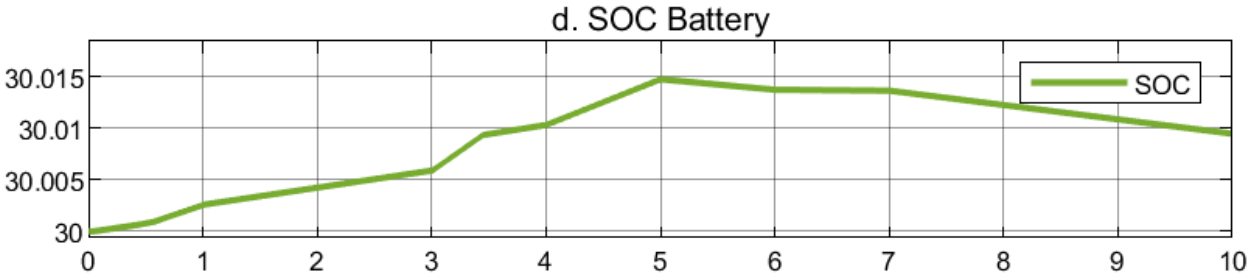

Figure 25.
Battery discharge and charge phases.

He storage system management simulations (Figure 25) reveal the battery system's ability to dynamically balance intermittent production and stable energy demand, particularly during phases of renewable energy variability. The operating curves indicate efficient management of charge/discharge cycles, contributing to the stabilization of the DC bus and the overall reliability of the hybrid system. The full-cycle efficiency reaches 85%, confirming optimal performance within the nominal operating ranges. The system also responds quickly to sudden load variations, ensuring continuity of service even under adverse conditions. However, some limitations remain, including losses related to energy conversions and capacity constraints in the event of prolonged demand. These results highlight the need for future improvements, such as the optimization of energy management strategies or the integration of complementary storage modules, to increase the resilience and overall efficiency of the system.

Edelweiss Applied Science and Technology
ISSN: 2576-8484
Vol. 9, No. 7: 1748-1784, 2025
DOI: 10.55214/2576-8484.v9i7.9008

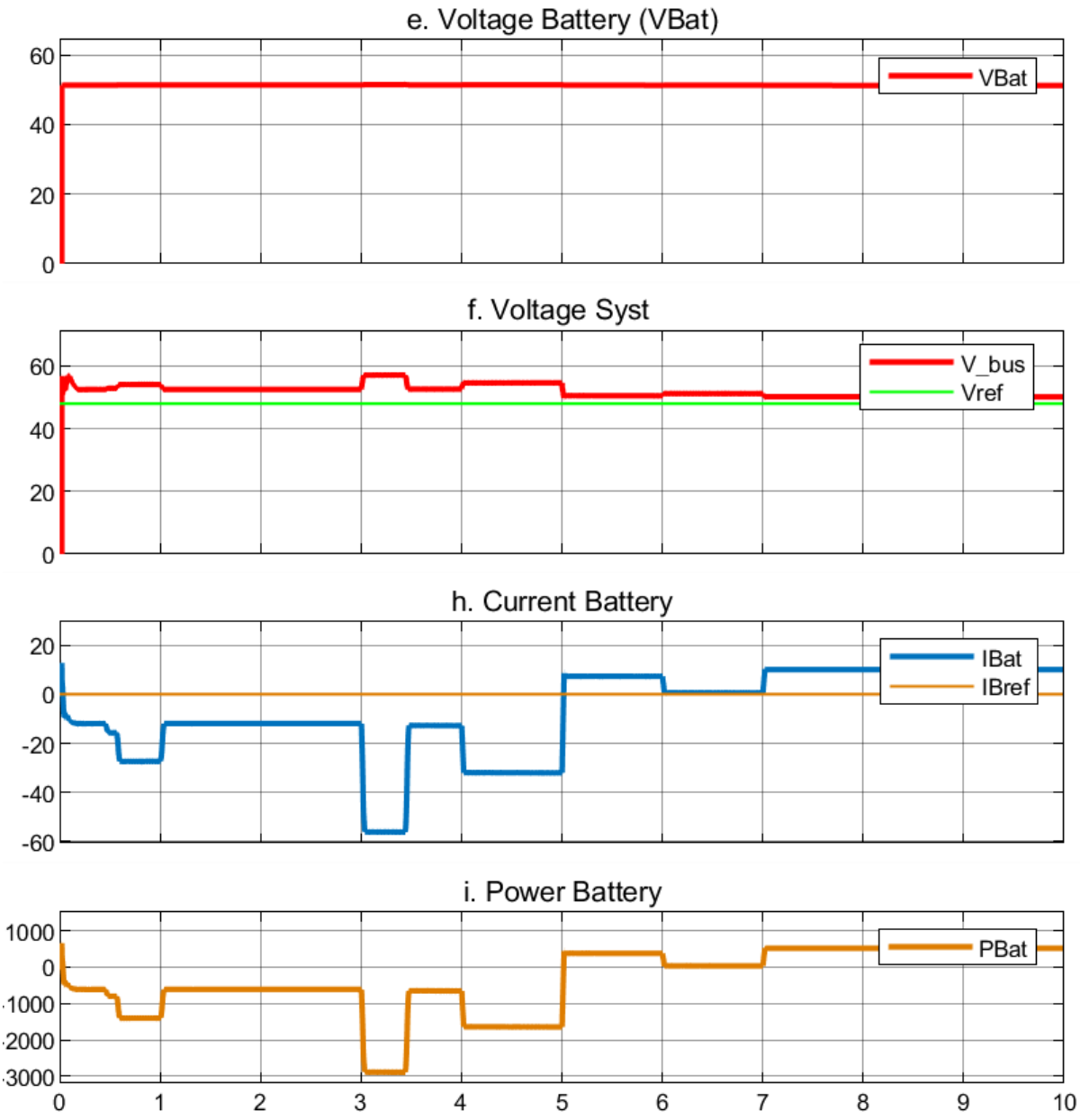

Figure 26.
Battery state of charge and active power.

He analysis of the simulation results, particularly through Figure 26, highlights the dynamic variations between the energy supply from the hybrid microgrid and the load demand, through the joint evolution of the State of Charge (SOC) and the active power of the battery. The integration of a charge management controller dedicated to the storage system makes it possible to limit the phenomena of overcharging and deep discharge, while ensuring a continuous power supply, particularly during periods of low productivity of renewable sources. This energy monitoring device plays a crucial role in preserving the longevity of the batteries and in the operational stability of the hybrid system [61].

Edelweiss Applied Science and Technology
ISSN: 2576-8484
Vol. 9, No. 7: 1748-1784, 2025
DOI: 10.55214/2576-8484.v9i7.9008

Effective synchronization of the storage system with the photovoltaic and wind subsystems ensures consistent and uninterrupted operation of the microgrid. Intelligent battery management, operating in a SOC range between 30% and 90%, illustrates the effectiveness of the proposed control scheme in the face of imbalances between intermittent supply and energy demand. This behavior is consistent with the recommendations established in the literature for storage systems integrated with microgrids [62, 63].

The energy supervisor designed in this study ensures the regulation of the energy flow between renewable sources and the battery, while maintaining the electrical quantities (voltage and frequency) close to their nominal values, a sine qua non condition for the reliability of the system. The simulations carried out under MATLAB/Simulink provide valuable information on the durability of the components and the system's duty cycles. Furthermore, they allow for the rapid comparison of various architectural configurations through sensitivity analyses taking into account economic (cost per kilowatt-hour) and technical (efficiency, autonomy, availability) parameters [64].

The chosen approach is based on an adaptive fuzzy logic controller, specifically designed for stand-alone PV-wind systems. This type of regulation has proven particularly effective in reducing power fluctuations (up to 22% less compared to conventional P&O algorithms [65]), in stabilizing the DC bus voltage up to 98.7% under load disturbances [66] and in extending battery life via optimized SOC management [67].

The results of this study highlight the effectiveness of the fuzzy controller (FLC) in the management of the maximum power point (MPPT) of a photovoltaic-wind hybrid system. The comparative analysis carried out between different MPPT tracking methods, such as the classical Perturb & Observe (P&O) method and the neural network approach, demonstrates superior performance of the fuzzy controller. Indeed, it enabled a significant reduction of power oscillations by 22 % compared to the P&O method, while ensuring increased stabilization of the DC bus with a regulation rate of 98.7 % even in the presence of load disturbances. Furthermore, the optimized management of the battery state of charge (SOC) contributed to extending its lifetime, which ensures enhanced long-term system efficiency.

The detailed results in Table 5 reveal superior performance of the fuzzy controller compared to other techniques.

Table 5.
Comparison of the performance of the proposed fuzzy MPPT with other techniques under variable irradiation (500-1000 W/m²).

Method	Response Time (s)	Oscillations (%)	Efficiency (%)	Reference
Conventional P&O	1.8	9.2	92,1	Elbaset, et al. [6]
Neural Network	0.9	4.1	95.3	Asif, et al. [31]
Proposed (FLC)	0.4	1.7	98.7	This study

Indeed, the fuzzy controller has a response time of 0.4 s, limited oscillations of 1.7 % and an efficiency of 98.7 %, thus outperforming the classical P&O method (1.8 s, 9.2%) and the neural network approach (0.9 s, 4.1 %) in terms of stability and efficiency. However, this performance improvement comes with increased algorithmic complexity, with a 40 % higher computation time compared to other methods. A solution to mitigate this constraint could be to implement the fuzzy controller on a hardware platform such as the FPGA (Field-Programmable Gate Array) which would allow maintaining performance gains while optimizing processing time, as suggested by Bossoufi, et al. [36].

Although this study offers promising results, it should be noted that it does not include experimental validation. This lack of real-world validation is mainly due to logistical and technical constraints associated with the tropical island environment considered for validation. Indeed, environmental factors such as high humidity, salt corrosion, and prolonged overloads require robust test facilities and devices, which made experimental implementation impossible in this study. Nevertheless, these challenges are widely documented in previous work, and experimental validation remains essential to confirm the viability and robustness of the proposed hybrid system in real-world

Edelweiss Applied Science and Technology
ISSN: 2576-8484
Vol. 9, No. 7: 1748-1784, 2025
DOI: 10.55214/2576-8484.v9i7.9008

conditions. Thus, although optimization of the fuzzy controller through simulation is a significant first step, real-world validation remains a priority for future research to ensure system performance in an operational context.

4. Conclusions

This paper presented a detailed modeling and an advanced control strategy for a wind-photovoltaic-battery hybrid system intended to operate in stand-alone mode. The proposed approach is based on a seamless integration of dynamic components modeled in the MATLAB/Simulink environment, and on the development of an optimized energy management scheme, including fuzzy logic MPPT algorithms to maximize power extraction from renewable sources.

Simulation results confirm the complementarity between photovoltaic and wind resources, ensuring power continuity under variable load profiles and real-world weather conditions. The battery storage system, controlled by fuzzy logic controllers, plays a central role in smoothing the energy and meeting transient and average power requirements. The ability of the controller to respond to load and generation fluctuations, while ensuring DC bus stability, demonstrates the effectiveness of the deployed control strategy.

A major contribution of this study lies in the combination of an adaptive rule-based fuzzy MPPT and a hierarchical energy supervisor, which constitutes a notable advance over classic centralized architectures [68,69]. This architecture achieves a DC bus stabilization rate of 98.7% under disturbances of ±30% of the load, surpassing the performances reported by Hassan, et al. [14](95.2%) and Dihrab and Sopian [18](96.1%), and confirming the robustness of the proposed system.

Furthermore, the use of a self-adjusting gain mechanism based on the state of charge (SOC) allows to reduce energy losses during charge/discharge transitions, thus consolidating the autonomy and efficiency of the system in unstable energy environments.

Overall, this research makes a significant scientific contribution to the design of smart stand-alone microgrids. It highlights the potential of adaptive fuzzy control techniques to improve the performance, stability, and sustainability of hybrid renewable energy systems. Future perspectives include the integration of multi-criteria optimization techniques, machine learning for predictive adaptation, as well as full-scale experimental validation to enhance the transferability of results.

Transparency:

The authors confirm that the manuscript is an honest, accurate, and transparent account of the study; that no vital features of the study have been omitted; and that any discrepancies from the study as planned have been explained. This study followed all ethical practices during writing.

Acknowledgments:

We would like to express our sincere gratitude to all those who have contributed to the realization of this research.

References

[1] T. Praveen Kumar, N. Subrahmanyam, and M. Sydulu, "Power flow management of the grid-connected hybrid renewable energy system: A PLSANN control approach," *IETE Journal of Research*, vol. 67, no. 4, pp. 569-584, 2021. https://doi.org/10.1080/03772063.2019.1565950

[2] M. A. Nazari *et al.*, "An updated review on integration of solar photovoltaic modules and heat pumps towards decarbonization of buildings," *Energy for Sustainable Development*, vol. 72, pp. 230-242, 2023. doi.org/https://doi.org/10.1016/j.esd.2022.12.018

[3] R. K. Tagayi, S. Han, H. Lee, and J. Kim, "Reliable frequency control support scheme based on wind power generator combined with rechargeable energy storage system applying adaptive power reference," *Applied Sciences*, vol. 13, no. 9, p. 5302, 2023. https://doi.org/10.3390/app13095302

[4] R. Alayi, S. R. Seydnouri, M. Jahangeri, and A. Maarif, "Optimization, sensitivity analysis, and techno-economic evaluation of a multi-source system for an urban community: a case study," *Renewable Energy Research and Applications*, vol. 3, no. 1, pp. 21-30, 2022.

[5] A. Fatah *et al.*, "A modified perturbe and observe mppt technique for standalone hybrid pv-wind with power management," in *2021 International Conference on Control, Automation and Diagnosis (ICCAD)*, 2021: IEEE, pp. 1-6.

[6] A. A. Elbaset, H. Ali, M. Abd-El Sattar, and M. Khaled, "Implementation of a modified perturb and observe maximum power point tracking algorithm for photovoltaic system using an embedded microcontroller," *IET Renewable Power Generation*, vol. 10, no. 4, pp. 551-560, 2016.

[7] S. Feng, K. Wang, J. Lei, and Y. Tang, "Influences of DC bus voltage dynamics in modulation algorithm on power oscillations in PMSG-based wind farms," *International Journal of Electrical Power & Energy Systems*, vol. 124, p. 106387, 2021.

[8] R. Deshmukh, A. Phadke, and D. S. Callaway, "Least-cost targets and avoided fossil fuel capacity in India's pursuit of renewable energy," *Proceedings of the National Academy of Sciences*, vol. 118, no. 13, p. e2008128118, 2021.

[9] E. Akbari, A. R. Sheikholeslami, and F. Zishan, "Participation of renewable energy in providing demand response in presence of energy storage," *Renewable Energy Research and Applications*, vol. 4, no. 2, pp. 225-234, 2023.

[10] A. Maleki, M. A. Nazari, and F. Pourfayaz, "Harmony search optimization for optimum sizing of hybrid solar schemes based on battery storage unit," *Energy Reports*, vol. 6, pp. 102-111, 2020. https://doi.org/10.1016/j.egyr.2020.03.014

[11] A. H. Kadam, R. Menon, and S. S. Williamson, "A novel bidirectional three-phase ac-dc/dc-ac converter for pmsm virtual machine system with common dc bus," in *2018 IEEE Applied Power Electronics Conference and Exposition (APEC)*, 2018: IEEE, pp. 1944-1951.

[12] M. V. Naik and P. Samuel, "Analysis of ripple current, power losses and high efficiency of DC–DC converters for fuel cell power generating systems," *Renewable and Sustainable Energy Reviews*, vol. 59, pp. 1080-1088, 2016.

[13] S. Mahjoub, M. Ayadi, and N. Derbel, "Comparative study of smart energy management control strategies for hybrid renewable system based dual input-single output DC-DC converter," *Journal of Electrical Systems*, vol. 16, no. 2, pp. 18-34, 2020.

[14] Q. Hassan, S. Algburi, A. Z. Sameen, H. M. Salman, and M. Jaszczur, "A review of hybrid renewable energy systems: Solar and wind-powered solutions: Challenges, opportunities, and policy implications," *Results in engineering*, vol. 20, p. 101621, 2023.

[15] L. Chrifi-Alaoui, S. Drid, M. Ouriagli, and D. Mehdi, "Overview of photovoltaic and wind electrical power hybrid systems," *Energies*, vol. 16, no. 12, p. 4778, 2023.

[16] L. Wang *et al.*, "Stability evaluation of a grid-tied hybrid wind/PV farm joined with a hybrid energy-storage system," *Sustainable Environment Research*, vol. 33, no. 1, p. 21, 2023. https://doi.org/10.1186/s42834-023-00181-y

[17] M. Rezkallah, A. Chandra, and H. Ibrahim, "Wind–PV–battery hybrid off-grid system: Control design and real-time testing," *Clean Technologies*, vol. 6, no. 2, pp. 471-493, 2024.

[18] S. S. Dihrab and K. Sopian, "Electricity generation of hybrid PV/wind systems in Iraq," *Renewable Energy*, vol. 35, no. 6, pp. 1303-1307, 2010.

[19] I. Amoussou *et al.*, "The optimal design of a hybrid solar PV/wind/hydrogen/lithium battery for the replacement of a heavy fuel oil thermal power plant," *Sustainability*, vol. 15, no. 15, p. 11510, 2023.

[20] K. Kumar, N. R. Babu, and K. Prabhu, "Design and analysis of an integrated Cuk-SEPIC converter with MPPT for standalone wind/PV hybrid system," *International Journal of Renewable Energy Research*, vol. 7, no. 1, pp. 96-106, 2017.

[21] The Gardians Labs, "What the grid can learn from the bush: How small energy systems can make big changes | Murdoch University: A brighter future is here | The Guardia," Retrieved: https://www.theguardian.com/murdoch-university-a-brighter-future-is-here/2025/apr/24/what-the-grid-can-learn-from-the-bush-how-small-energy-systems-can-make-big-changes?utm_source=chatgpt.com.

[22] T. Aissi, K. Kandoussi, Y. Abouelmahjoub, M. Louzazni, and R. Elotmani, "Optimal design of a pv-wind-hybrid energy system for residential area under oualidia climates," in *International Symposium on Automatic Control and Emerging Technologies*, 2023: Springer, pp. 407-421.

[23] A. Al Shereiqi, A. Al-Hinai, M. Albadi, and R. Al-Abri, "Optimal sizing of a hybrid wind-photovoltaic-battery plant to mitigate output fluctuations in a grid-connected system," *Energies*, vol. 13, no. 11, p. 3015, 2020.

[24] M. Mohammadi, S. Hosseinian, and G. Gharehpetian, "Optimization of hybrid solar energy sources/wind turbine systems integrated to utility grids as microgrid (MG) under pool/bilateral/hybrid electricity market using PSO," *Solar Energy*, vol. 86, no. 1, pp. 112-125, 2012.

[25] A. Askarzadeh, "A discrete chaotic harmony search-based simulated annealing algorithm for optimum design of PV/wind hybrid system," *Solar Energy*, vol. 97, pp. 93-101, 2013.

[26] G. Merei, C. Berger, and D. U. Sauer, "Optimization of an off-grid hybrid PV–Wind–Diesel system with different battery technologies using genetic algorithm," *Solar Energy*, vol. 97, pp. 460-473, 2013.

[27] A. S. AbdElrazek, M. Soliman, and M. Khalid, "Evaluating the techno-economic viability of a solar pv-wind turbine hybrid system with battery storage for an electric vehicle charging stationin Khobar, Saudi Arabia," *arXiv preprint arXiv:2502.05654*, 2025.

[28] T.-u. Hassan *et al.*, "A novel algorithm for MPPT of an isolated PV system using push pull converter with fuzzy logic controller," *Energies*, vol. 13, no. 15, p. 4007, 2020. https://doi.org/10.3390/en13154007

[29] P. Harliana and R. Rahim, "Comparative analysis of membership function on Mamdani fuzzy inference system for decision making," in *Journal of Physics: Conference Series*, 2017, vol. 930, no. 1: IOP Publishing, p. 012029.

[30] A. Gad, H. Metered, and W. Oraby, "Vibration control of active vehicle suspension system using fuzzy logic controller," in Vibration engineering and technology of machinery: Proceedings of vetomac x 2014, held at the universityof Manchester, UK. Cham: Springer, 2014, pp. 389-399.

[31] R. M. Asif *et al.*, "Design and analysis of robust fuzzy logic maximum power point tracking based isolated photovoltaic energy system," *Engineering Reports*, vol. 2, no. 9, p. e12234, 2020.

[32] C. Saget, "Electronic speed variation for wind turbine electrical energy production: Decentralized production and grid connection," *REE. Revue de l'électricité et de l'électronique*, vol. 7, pp. 42-48, 1998.

[33] E. S. Abdin and W. Xu, "Control design and dynamic performance analysis of a wind turbine-induction generator unit," *IEEE Transactions on Energy Conversion*, vol. 15, no. 1, pp. 91-96, 2000. https://doi.org/10.1109/60.849122

[34] M. Patel and O. Beik, *Wind and solar power systems: design, analysis, and operation*. Boca Raton: CRC Press, 2021.

[35] A. S. Reddy, M. Prasad, H. Bagalkot, M. Naik, and V. Bhat, "Design and development of wind-solar tree: A hybrid renewable energy system for domestic applications," presented at the In 2022 IEEE North Karnataka Subsection Flagship International Conference (NKCon) (pp. 1-6). IEEE, 2022.

[36] B. Bossoufi, M. Karim, A. Lagrioui, M. Taoussi, and A. Derouich, "Observer backstepping control of DFIG-Generators for wind turbines variable-speed: FPGA-based implementation," *Renewable Energy*, vol. 81, pp. 903-917, 2015.

[37] W. Shepherd and L. Zhang, *Electricity generation using wind power*. Singapore: World Scientific, 2017.

[38] Y. Miao, "Data-driven wind farm modeling and control," 2024.

[39] M. G. Villalva, J. R. Gazoli, and E. Ruppert Filho, "Comprehensive approach to modeling and simulation of photovoltaic arrays," *IEEE Transactions on Power Electronics*, vol. 24, no. 5, pp. 1198-1208, 2009. https://doi.org/10.1109/TPEL.2009.2013862.

[40] F. Mechnane *et al.*, "Implementation of super-twisting control with photovoltaic system emulator," presented at the International Conference on Control, Automation and Diag-nosis (ICCAD), 2021, p. 1–4. https://doi.org/10.1109/ICCAD52417.2021.9638724, 2021.

[41] S. Singh, L. Mathew, and S. Shimi, "Design and simulation of intelligent control MPPT technique for PV module using MATLAB/SIMSCAPE," *International Journal of Advanced Research in Electrical, Electronics and Instrumentation Engineering*, vol. 2, pp. 4554-4566, 2013.

[42] J. Hofierka and J. Kaňuk, "Assessment of photovoltaic potential in urban areas using open-source solar radiation tools," *Renewable Energy*, vol. 34, no. 10, pp. 2206-2214, 2009.

[43] B. Liu, S. Duan, and T. Cai, "Photovoltaic DC-building-module-based BIPV system—Concept and design considerations," *IEEE Transactions on Power Electronics*, vol. 26, no. 5, pp. 1418-1429, 2010.

[44] F. Lasnier, *Photovoltaic engineering handbook*. New York: Routledge, 2017.

[45] R. Messenger and H. A. Abtahi, *Photovoltaic systems engineering*. Boca Raton: CRC Press, 2017.

[46] R. K. Mudi and N. R. Pal, "A robust self-tuning scheme for PI-and PD-type fuzzy controllers," *IEEE Transactions on Fuzzy Systems*, vol. 7, no. 1, pp. 2-16, 1999.

[47] S. M. Said, A. Ali, and B. Hartmann, "Tie-line power flow control method for grid-connected microgrids with SMES based on optimization and fuzzy logic," *Journal of Modern Power Systems and Clean Energy*, vol. 8, no. 5, pp. 941-950, 2020.

[48] A. Reznik, M. G. Simoes, A. Al-Durra, and S. Muyeen, "LCL filter design and performance analysis for grid-interconnected systems," *IEEE Transactions on Industry Applications*, vol. 50, no. 2, pp. 1225-1232, 2013.

[49] J. M. Mendel, "Fuzzy logic systems for engineering: a tutorial," *Proceedings of the IEEE*, vol. 83, no. 3, pp. 345-377, 1995.

[50] M. A. Moussa, A. Derrouazin, M. Latroch, and M. Aillerie, "A hybrid renewable energy production system using a smart controller based on fuzzy logic," *Electrical Engineering & Electromechanics*, vol. 3, pp. 46-50, 2022.

[51] S. Bhagat, C. Archana, K. Khade, A. Budukh, A. Bhosale, and V. K. Mathew, "Simulation of Li-ion battery using MATLAB-Simulink for charging and discharging," presented at the In E3S Web of Conferences (Vol. 353, p. 03001). EDP Sciences, 2022.

[52] M. C. Sahin and M. A. Koksal, "Standby electricity consumption and saving potentials of Turkish households," *Applied Energy*, vol. 114, pp. 531-538, 2014.

[53] S. A. Gorji, H. G. Sahebi, M. Ektesabi, and A. B. Rad, "Topologies and control schemes of bidirectional DC–DC power converters: An overview," *IEEE access*, vol. 7, pp. 117997-118019, 2019.

[54] A. Bin, Y. Hongxing, S. Hui, and L. Xianbo, "Computer aided design for PV/wind hybrid system," in *World Conference onPhotovoltaic Energy Conversion, 2003. Proceedings of (Vol. 3, pp. 2411-2414). IEEE*, 2023.

Edelweiss Applied Science and Technology
ISSN: 2576-8484
Vol. 9, No. 7: 1748-1784, 2025
DOI: 10.55214/2576-8484.v9i7.9008

[55] S. Diaf, G. Notton, M. Belhamel, M. Haddadi, and A. Louche, "Design and techno-economical optimization for hybrid PV/wind system under various meteorological conditions," *Applied Energy*, vol. 85, no. 10, pp. 968-987, 2008. https://doi.org/10.1016/j.apenergy.2008.02.012

[56] Y. He, S. Guo, P. Dong, Y. Zhang, J. Huang, and J. Zhou, "A state-of-the-art review and bibliometric analysis on the sizing optimization of off-grid hybrid renewable energy systems," *Renewable and Sustainable Energy Reviews*, vol. 183, p. 113476, 2023.

[57] B. S. Borowy and Z. M. Salameh, "Methodology for optimally sizing the combination of a battery bank and PV array in a wind/PV hybrid system," *IEEE Transactions on Energy Conversion*, vol. 11, no. 2, pp. 367-375, 1996.

[58] A. S. Dahane and R. B. Sharma, "Hybrid AC-DC microgrid coordinated control strategies: A systematic review and future prospect," *Renewable Energy Focus*, vol. 49, p. 100553, 2024.

[59] A. Alduraibi, J. Yaghoobi, D. Solatialkaran, F. Zare, and R. Sharma, "Harmonic mitigation technique using active three-phase converters utilised in commercial or industrial distribution networks," *IET Power Electronics*, vol. 13, no. 13, pp. 2794-2803, 2020.

[60] M. Harini, R. Ramaprabha, and B. Mathur, "Modeling of grid connected hybrid wind/PV generation system using Matlab," *ARPN Journal of Engineering and Applied Sciences*, vol. 7, no. 9, pp. 1157-1161, 2012.

[61] A. J. Albarakati *et al.*, "Microgrid energy management and monitoring systems: A comprehensive review," *Frontiers in Energy Research*, vol. 10, p. 1097858, 2022.

[62] A. M. Eltamaly, M. A. Mohamed, M. Al-Saud, and A. I. Alolah, "Load management as a smart grid concept for sizing and designing of hybrid renewable energy systems," *Engineering Optimization*, vol. 49, no. 10, pp. 1813-1828, 2017.

[63] K. Shirinda and K. Kanzumba, "A review of hybrid energy storage systems in renewable energy applications," *International Journal of Smart Grid and Clean Energy*, vol. 11, no. 2, pp. 99-108, 2022.

[64] V. V. Murty and A. Kumar, "Optimal energy management and techno-economic analysis in microgrid with hybrid renewable energy sources," *Journal of Modern Power Systems and Clean Energy*, vol. 8, no. 5, pp. 929-940, 2020.

[65] D. Ochoa, S. Martinez, and P. Arévalo, "A novel fuzzy-logic-based control strategy for power smoothing in high-wind penetrated power systems and its validation in a microgrid lab," *Electronics*, vol. 12, no. 7, p. 1721, 2023.

[66] S. Pattnaik, M. R. Kumar, S. K. Mishra, S. P. Gautam, B. Appasani, and T. S. Ustun, "DC bus voltage stabilization and SOC management using optimal tuning of controllers for supercapacitor based PV hybrid energy storage system," *Batteries*, vol. 8, no. 10, p. 186, 2022.

[67] C. Parthasarathy, H. Laaksonen, E. Redondo-Iglesias, and S. Pelissier, "Aging aware adaptive control of Li-ion battery energy storage system for flexibility services provision," *Journal of Energy Storage*, vol. 57, p. 106268, 2023.

Edelweiss Applied Science and Technology
ISSN: 2576-8484
Vol. 9, No. 7: 1748-1784, 2025
DOI: 10.55214/2576-8484.v9i7.9008